

**Precipitation of anion inclusions and plasticity under hydrostatic pressure in II-VI crystals**

G. P. Lindberg\* and B. A. Weinstein†

*Department of Physics, SUNY at Buffalo, 239 Fronczak, Buffalo, New York 14260-1500, USA*

(Received 18 April 2016; revised manuscript received 25 July 2016; published 6 October 2016)

Precipitation of anion nanocrystals (NCs) in initially stoichiometric II-VI crystals under hydrostatic pressure and light exposure is explored by Raman spectroscopy, and the mechanism for this effect is analyzed by model calculations. ZnSe, ZnTe, and CdSe crystals are studied in bulk and/or epitaxial-film forms. Se and Te NCs in the trigonal (t) phase precipitate in ZnSe and ZnTe, but the effect is absent or minimal in CdSe. The precipitation is induced by pressure *and* assisted by sub-band-gap light. In ZnSe, t-Se NCs appear for pressure exceeding 4.8 GPa and light flux above 50–70 W/mm<sup>2</sup>. In ZnTe, the precipitation of t-Te NCs requires less pressure to initiate, and there is a clear upper-pressure limit for t-Te nuclei to form. We find also that ZnTe samples with cleavage damage or elevated zinc-vacancy content are more prone to form t-Te NCs at lower pressures (even 1 atm in some cases) and lower flux. The precipitation seen in ZnSe and ZnTe occurs at pressures far below their phase transitions, and cannot be due to those transitions. Rather, we propose that the NCs nucleate on dislocations that arise from hydrostatic-pressure induced plastic flow triggered by noncubic defect sites. Calculations of the kinetic barrier for growth of an optimally shaped nucleus are performed, including hydrostatic pressure in the energy minimization scheme. Using sensible values for the model parameters related to the cohesive energies of Se and Te, the calculations account for our main observations, including the existence of an upper pressure limit for precipitation, and the absence of precipitation in CdSe. We consider the effects of pressure-induced precipitate formation on the I-II phase transitions in a variety of binary semiconductors and make predictions of when this effect should be important.

DOI: [10.1103/PhysRevB.94.134102](https://doi.org/10.1103/PhysRevB.94.134102)**I. INTRODUCTION**

The effects of applied hydrostatic pressure on crystals can be much more complex than the standard elastic-compression-phase-transition scenario. Crystal defects introduce disorder that can change under pressure. For defects that are photoactive the changes can be sensitive to light. These effects often are assumed to be small if the initial concentration of defects is low. This paper challenges that assumption.

We focus here on three II-VI semiconductors—ZnSe, ZnTe, and CdSe, all grown in the zincblende (ZB) phase as high-quality bulk crystals and/or epitaxial films. Raman spectroscopy is used to probe the structural and chemical disorder that develops under external pressure. It is evident that *plastic deformation* plays a prominent role. The ZB structure is tetrahedral with a single bond type, so one usually does not consider plastic deformation for the pressure-induced changes in phase I (stable ambient phase). However, this relies on modeling the crystal by its ideal lattice in the elastic regime. For real crystals the situation can be different, and when pressure-induced plasticity leads to structural and chemical disorder in phase I, one should expect related impacts on the I-II phase transition as well.

The dependence on pressure of the phonon Raman spectra in ZnSe [1–5], ZnTe [1,6–8], and CdSe [in its wurtzite (WZ) and its nanocrystal ZB forms] [9–12], and in related Zn<sub>1-x</sub>M<sub>x</sub>Se (M = Cd, Mn, Fe, Co) alloys [13–19], have been measured by many groups (see Ref. [20] for a review of early work). In parallel, semiempirical [21,22] and *ab initio* [23–29]

calculations have yielded a microscopic picture of the effects of pressure on the phonon properties of these crystals in the elastic limit. The high pressure phase changes are explored in many of the Raman studies and calculations [30–37], as well as in numerous high-pressure x-ray experiments on single crystals and powders [4,38–44]. As a result, the sequence of equilibrium phases in ZnSe, ZnTe, and CdSe are well known [45,46] (see Table I).

Experiments in which applied pressure introduces structural and/or chemical disorder are prone to misinterpretation. For example, in GaAs, a detailed study of the I-II phase transition by Besson *et al.* [47] found that bond coordination, nearest-neighbor distance, and crystal symmetry each change at different pressures, accompanied by related formation of point defects, twinning, and amorphous-crystalline mixtures. This blurs the phase boundary, and makes its measurement by different methods confusing, especially in the hysteresis region between the forward and reverse transitions. Of particular relevance here, in ZnSe, ZnTe, and several ZnM<sub>x</sub>Se<sub>1-x</sub> (M = Cd, Mn, Fe; 0 < x < 0.33) alloys, some studies observed anomalous Raman peaks that, although absent in the as-grown samples, appeared at pressures much below the I-II transition and had large negative pressure shifts [6,13,15–18,48,49]. Different works reported the peaks before and/or after the transitions in bulk crystals, powdered crystals, epitaxial films, and nanoparticles. These spectral features were either left unassigned, misinterpreted as due to unknown low-pressure phases [15–18,48,49], or attributed to metastable post-transition phases in, e.g., the cinnabar or wurtzite structures [6,13].

Anomalous Raman peaks also were observed during an initial Raman study on ZnSe and ZnTe vapor-grown crystals under applied pressure in our laboratory [8]. The strange peaks had frequencies and negative pressure shifts comparable to

\*Present address: Rochester Precision Optics, LLC, W. Henrietta, NY 14586, USA.

†Corresponding author: phyberni@buffalo.edu

TABLE I. Samples studied in this work, and some relevant material properties.

Sample	Fabrication	Pressures studied (GPa)	I-II change in structure <sup>a</sup>	I-II $P_I$ (GPa) <sup>a</sup>	$E_g$ (eV) vs $P$ (GPa)	$B_0$ (GPa) <sup>b</sup>	$\mu$ (GPa) <sup>b</sup>
<sup>68</sup> Zn <sup>76</sup> Se	Bulk crystals (Ar transp.) <sup>c</sup>	0–12.5	ZB-NaCl	13.0	$(2.70 + 0.072P - 0.0015P^2)^d$	62.4	32.9
<sup>64</sup> Zn <sup>nat</sup> Te	Bulk crystals (Ar transp.) <sup>c</sup>	0–6.5	ZB-cinnabar	9.5	$(2.28 + 0.11P - 0.005P^2)^e$	51	24.8
ZnTe/GaSb film I	MBE, 2.5 $\mu$ m thick BEP Zn : Te $\sim$ 1.2 : 1 <sup>f</sup>	0–8.5	ZB-cinnabar	9.5	$(2.28 + 0.11P - 0.005P^2)^e$	51	24.8
ZnTe/GaSb film II	MBE, 2.5 $\mu$ m thick BEP Zn : Te $\sim$ 1.0 : 1 <sup>f</sup>	0–8.5	ZB-cinnabar	9.5	$(2.28 + 0.11P - 0.005P^2)^e$	51	24.8
CdSe/GaAs with ZB-CdSe	MBE, 0.5 $\mu$ m thick BEP Cd : Se $\sim$ 0.4 : 1 <sup>g</sup>	0–7.0	WZ-NaCl ZB-NaCl	2.5 3.1, <sup>h</sup> 3.0 <sup>i</sup>	$(1.67 + 0.048P - 0.002P^2)^{g,j}$	55.7	13.6

<sup>a</sup>Reference [45] and references therein.

<sup>b</sup>Reference [65] and references therein; for CdSe  $B_0$  and  $\mu$  of the wurtzite phase are used.

<sup>c</sup>Reference [59].

<sup>d</sup>Reference [62].

<sup>e</sup>Reference [63].

<sup>f</sup>Reference [60].

<sup>g</sup>Reference [61].

<sup>h</sup>This work.

<sup>i</sup>References [10], for 45A NCs.

<sup>j</sup>Reference [64].

those found by earlier workers, and from those properties could be assigned to the A1 breathing modes of crystalline (trigonal) Se and Te. The results suggested that Se and Te nanocrystals (NCs) could be made to *precipitate within otherwise stoichiometric* II-VI hosts under applied hydrostatic pressure *and* exposure to sub-band-gap light. The required ranges of pressure and photon flux differed in the two Zn-chalcogenides, and other results on CdSe were indeterminate as to whether Se NCs formed. The mechanisms for the NC precipitation, and the differences in ZnSe, ZnTe, and CdSe, were not understood in this brief work [8], except to speculate that macroscopic defects and Zn diffusion might somehow be involved.

Other experiments, on ZnSe nanoparticles prepared by mechanical milling of elemental Zn and Se, also observed Se inclusions [4]. Unlike our results on single crystals, the Se Raman signature appeared in the 1 atm spectra as well as at elevated pressures. Consequently, the origin was thought to be incomplete mixing during milling. Grown-in inclusions are common in II-VI and III-V crystals prepared under less than ideal conditions [50–56]. However, incomplete mixing cannot explain why elemental inclusions form under pressure in *stoichiometric* high-quality crystals, as seen in our Raman experiments. A different mechanism must be operating.

The comprehensive study in this paper investigates the operation and physical basis of this mechanism. Experimental results and analysis are presented that provide answers to many of the questions raised in Ref. [8]. The most puzzling are the following. (i) What is the origin of the different pressure ranges for chalcogenide precipitation in ZnSe and ZnTe? Especially perplexing is the existence of an upper pressure limit, as clearly seen in ZnTe. (ii) What causes the differences in photon flux needed for precipitation? This shows sample-to-sample variation in ZnTe, as opposed to the more

defined onset level in ZnSe. (iii) Lastly, how can one account for the behavior in CdSe, for which NC precipitation is either absent or minimal? To resolve these issues here we present experimental results that investigate the NC precipitation in epitaxial ZnTe films with different Zn-vacancy contents; report detailed comparisons of the bulk spectra in ZnSe and in ZnTe that explore the roles of incident flux, laser wavelength, and mechanical (cleaving) damage; and characterize the defect contents in all of the bulk and film samples by luminescence spectroscopy. In addition, calculations are carried out based on a model of precipitate nucleation at dislocations due to Cahn [57,58], which we modify to include pressure. It will be seen that this treatment can account for the unexplained issues. Finally, we propose criteria to judge when pressure-induced precipitation could impact the I-II phase changes in a number of common semiconductors.

## II. SAMPLES AND EXPERIMENT

The studied samples are bulk crystals of <sup>68</sup>Zn<sup>76</sup>Se and <sup>64</sup>Zn<sup>nat</sup>Te, and thin films of ZnTe and CdSe deposited, respectively, on GaSb and GaAs substrates. The bulk and film samples were fabricated, respectively, in the laboratory of R. Lauck at the Max Planck Institute fur Festkörperforschung, and the laboratory of J. K. Furdyna and X. Liu at Notre Dame. All samples were grown in the zincblende (ZB) structure, under conditions that yield highly ordered closely stoichiometric single crystals. Table I summarizes the fabrication methods and some important properties that apply in the pressure ranges of our measurements. The bulk <sup>68</sup>Zn<sup>76</sup>Se and <sup>64</sup>Zn<sup>nat</sup>Te crystals are grown from the vapor phase using isotope-pure (96%–98%) starting materials [59]. For the <sup>64</sup>Zn<sup>nat</sup>Te sample, the ratio of Te isotopes is adjusted to match the natural average of 127.6 amu. The ZnTe and CdSe films are grown by molecular beam epitaxy (MBE), in an [001]

orientation, using conventional mixed-isotope sources. Two ZnTe films are studied. They are deposited using a different Zn:Te ratio in the beam equivalent pressure (BEP). For film I the BEP is 20% Zn rich, which tends to give material with a low density of Zn vacancies ( $V_{Zn}$ ); for film II the BEP ratio is 1:1, giving a higher  $V_{Zn}$  content. These  $\sim 2.5\text{-}\mu\text{m}$ -thick films are strain relaxed except near the GaSb interface. (The ZnTe-GaSb lattice mismatch is 0.13%; the critical thickness is  $\sim 180$  nm [66].) The CdSe MBE film is grown with the BEP ratio set in the Cd-deficient range found to optimize growth; its thickness is  $\sim 0.5$   $\mu\text{m}$ . Although CdSe is most commonly found in the wurtzite (WZ) phase at ambient conditions, Samarth *et al.* showed that robust high-quality ZB films can be fabricated by MBE on GaAs substrates [61]. The 7% lattice mismatch between CdSe and GaAs leads to a high density of misfit dislocations and some stacking faults in the interfacial region. However, on approaching the epilayer's free surface, these defects decrease in density appreciably, resulting in ZB-structure CdSe films with an unstrained cubic lattice constant.

Table I also lists the observed I-II structure changes in ZnSe, ZnTe, and CdSe, and their transition thresholds under increasing hydrostatic pressure [67]. The reverse transitions occur on decreasing pressure, but there is as much as 2–3 GPa hysteresis, and metastable phases can appear in the hysteresis regions (e.g., cinnabar in ZnSe [38,39] and wurtzite in ZnTe [6]). The latter findings can depend on experimental factors, such as the maximum up-stroke pressure, the presence of strain gradients, and whether single-crystal or powder samples are studied [47].

High-pressure Raman spectroscopy is carried out at room temperature (295 K) using a ruby-calibrated diamond-anvil cell (DAC) with hardened stainless steel gaskets and either 4:1 methanol:ethanol or 16:3:1 methanol:ethanol:water pressure media [20]. At 295 K these mixtures have static hydrostatic limits of 9.8 and  $\sim 11.5$  GPa, respectively [68]. Gasket holes  $\sim 200\text{--}300$   $\mu\text{m}$  diameter  $\times$  75  $\mu\text{m}$  deep form the sample chambers. DAC samples are prepared as approximate rectangular chips, cleaved from the growth materials and selected for size to ensure that no gasket pinching occurs; sample sizes are 100–150  $\mu\text{m}$  lateral  $\times$   $\sim 30$   $\mu\text{m}$  thick. The substrates of the ZnTe and CdSe films are thinned to 30  $\mu\text{m}$  (but not removed) before cleaving.

Raman spectra are recorded in backscattering using a 1 m double monochromator, and conventional photon counting or multichannel detection. Different  $\text{Kr}^+$  and  $\text{Ar}^+$  cw laser lines in the range 521–676 nm are employed for excitation, depending on the type of sample and the pressure of the measurement. Powers of 7–240 mW are focused to a  $\sim 35$   $\mu\text{m}$  diameter spot inside the DAC, giving flux densities on the samples of 5–175 W/mm<sup>2</sup> (including diamond reflection losses). For ZnSe and ZnTe, the Raman signals are excited using only sub-band-gap light in order to minimize laser heating, and probe primarily the interior of the samples. The choice of laser line depends on the shift with pressure of the fundamental band gap  $E_g(P)$ . The CdSe film stays opaque to the longest available wavelength 676 nm until the pressure exceeds 3 GPa; hence relatively low powers  $\leq 32$  mW are used for the CdSe experiments. The observed  $E_g(P)$  variations for these materials are also listed in Table I. Further measurement

details are given in the legends and captions of the figures in Sec. III.

*Defect characterization:* The Raman results presented in Sec. III develop evidence that plastic deformation resulting from the actions of applied hydrostatic pressure and laser exposure can cause precipitation of chalcogen NCs in II-VI crystals. To support this interpretation, it is important to characterize the defects in our samples, especially regarding: (i) any initial content of Se (Te) NCs, and (ii) the presence of defect sites that are locally noncubic. These low symmetry sites are important because they are sources of pressure-dependent internal shear strains that can promote generation and motion of lattice dislocations.

In order to gauge crystal quality and defect content, extensive ambient-pressure (1 atm) Raman and photoluminescence (PL) measurements using minimal laser power were recorded at 295 and 13 K, respectively. Examples of the one- and two-phonon 1 atm Raman spectra appear with the high-pressure data in Sec. III. As long as low laser power is used, the 1 atm spectra of the as-grown materials (measured on large crystals outside the DAC) show no anomalies. They exhibit sharp features with spectral positions and line shapes in accord with the established results for ZnSe, ZnTe, and CdSe [69–72], verifying the excellent single-crystal quality of the supplied material, and showing no evidence of grown-in Se (or Te) NCs.

The ambient-pressure PL spectra of our samples are presented and discussed with appropriate citations in Appendix A. The spectra reveal impurity and defect contents that are typical of high-quality ZnSe, ZnTe, and CdSe crystals grown by the vapor phase and MBE methods used in this work. Of particular relevance to the discussion in Sec. V, there is ample evidence for defects at noncubic local sites. The most important of these defects are Zn vacancies ( $V_{Zn}$ ), Cu impurities at cation ( $\text{Cu}_{Zn}$ ), or interstitial ( $\text{Cu}_I$ ) sites, near-neighbor pairs or clusters of such defects with shallow donors or with each other, and existing dislocations [73–75]. Generally, these imperfections produce deep levels, and sit at axially relaxed sites (usually trigonal or tetragonal in cubic hosts) as a result of Jahn-Teller distortions, proximity to other defects, or extended dislocation geometries [76].

### III. RESULTS

#### A. ZnSe

As described in Sec. I, puzzling issues were raised by the evidence in Ref. [8] that chalcogen NCs could form in ZnSe and ZnTe under various conditions of applied hydrostatic pressure and exposure to light. The Raman spectra in Figs. 1 and 2 highlight the changes that mark the onset of this effect in ZnSe, and directly compare spectra recorded at corresponding pressures using low and high laser powers. These results are important for understanding the precipitation mechanism, and are presented here to help focus the later discussion in Sec. IV.

The peak at  $210\text{cm}^{-1}$  in Fig. 1 is assigned by its frequency and pressure shift to the  $A_1$  mode of trigonal (t-) Se NCs [77,78]. These data, recorded at the 4.8 GPa threshold for precipitation in our  $^{68}\text{Zn}^{76}\text{Se}$  samples, show how the  $A_1$  peak appears and grows with time. Notice that

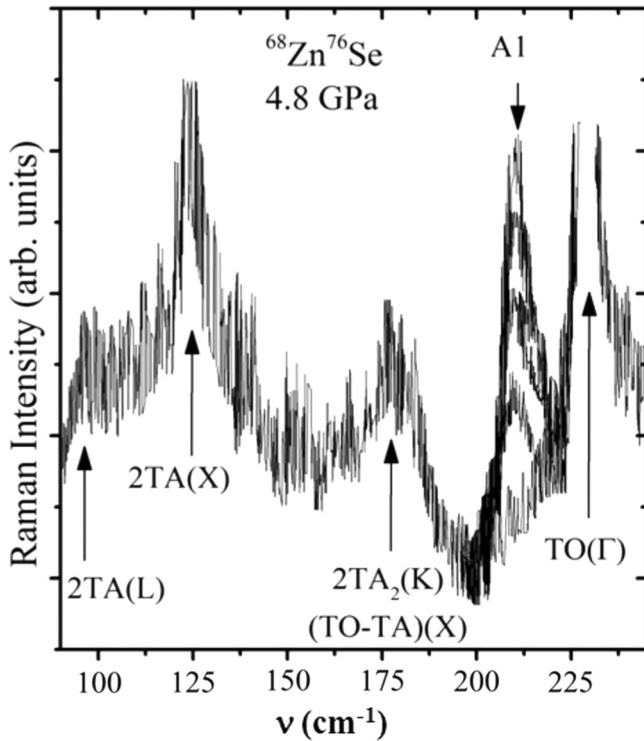


FIG. 1. Raman spectrum of  $^{68}\text{Zn}^{76}\text{Se}$  at 4.8 GPa and RT recorded using  $70\text{ W/mm}^2$ , 568 nm, cw laser flux. Five consecutive scans during 2.5 h are superimposed. The final plot is digitized for clarity of the t-Se A1 peak.

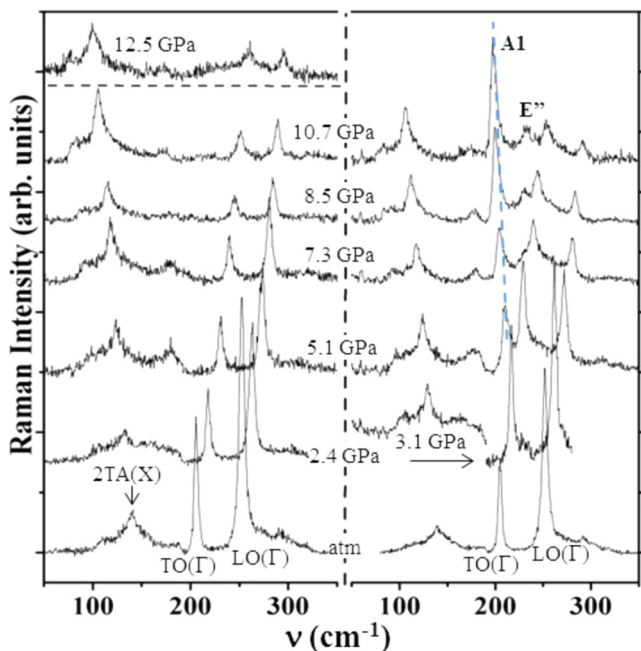


FIG. 2. Comparison of pressure-Raman spectra in  $^{68}\text{Zn}^{76}\text{Se}$  recorded using  $7\text{ W/mm}^2$  (left) and  $70\text{ W/mm}^2$  (right) laser flux at 568 nm. The sub-band-gap laser causes minimal heating. Right panel adapted from Ref. [8].

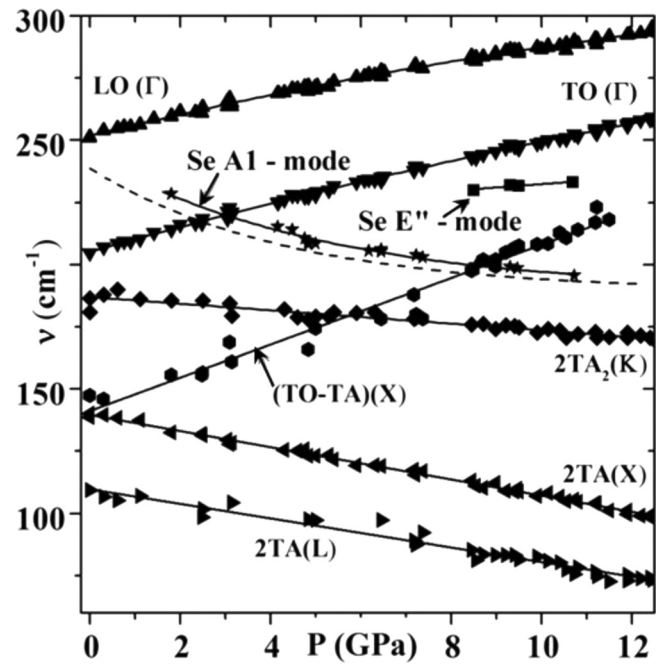


FIG. 3. Pressure shifts of Se A1 peak and nearby Raman features in  $^{68}\text{Zn}^{76}\text{Se}$ . Solid curves are best fits to our data. Dashed curve is explained in text.

only the A1 peak changes. The other spectral features arise from well-known [79] intrinsic one- and two-phonon modes in ZnSe (as labeled), and are unchanged in each of the five superimposed scans. The narrowness of the A1 peak implies that the Se NCs should be  $\geq 1\text{ nm}$  in diameter.

The precipitation of t-Se NCs in ZnSe also has a threshold in photon flux. Figure 2 summarizes the effects of both pressure and laser intensity on the  $^{68}\text{Zn}^{76}\text{Se}$  Raman spectra. It compares experiments on two cleaved chips in which intensities differing by a factor of 10 are used to record spectra at the same pressures (except 2.4 and 3.1 GPa). The low-power spectra show only intrinsic ZnSe modes. The same intrinsic features appear in the higher power data. *In addition*, above 4.8 GPa, we observe the t-Se A1 peak. At still higher pressures, this peak becomes the strongest feature in the spectrum [80], and a weak peak assigned to the  $E''$  mode of t-Se [77] also appears at frequencies just below  $\text{TO}(\Gamma)$ . On decreasing pressure (not shown), the A1 peak is observed until it is lost in overlap with the  $\text{LO}(\Gamma)$  peak at 1.8 GPa. For corresponding up- and down-cycle pressures the intrinsic ZnSe features show no appreciable changes.

The pressure shifts of the main spectral features in Fig. 2 are plotted in Fig. 3, including all the data on  $^{68}\text{Zn}^{76}\text{Se}$  for both laser powers. The intrinsic modes obey well-established trends [1,20]. However, the A1 peak (star symbols) exhibits a strong negative nonlinear pressure shift. The dashed curve gives the pressure shift of the t-Se A1 mode *in Se bulk crystals*, obtained from a fit to the collected data of Refs. [81–84]. This clearly shows the same variation as its ZnSe counterpart. In both cases, an exponential fit applies; Table II lists the best-fit coefficients. The small displacement between the dashed and solid curves ( $\sim 4.0\text{ cm}^{-1}$  at 2.8 GPa) arises from the Ref. [83] data, recorded without a pressure medium; omitting this data

TABLE II. Best fit to frequency vs pressure for Se and Te A1 peaks in crystals of t-Se and t-Te (from literature), and in ZnSe and ZnTe bulk samples (from present work.)

Fit parameters for $\nu(P) = \nu_0 + A \exp(-P/t_1)$		Se <sup>a,b,c,d</sup>	Te <sup>a,b,e</sup>
A1 (Lit.)	$\nu_0$	189(2)	102(3)
	$A$	49(2)	19(1)
	$t_1$	4.4(5)	2.7(5)
A1 (Present)	$\nu_0$	190(2)	101(3)
	$A$	55(2)	26(3)
	$t_1$	4.9(6)	2.3(6)

<sup>a</sup>Reference [83].

<sup>b</sup>Reference [81].

<sup>c</sup>Reference [84].

<sup>d</sup>Reference [82].

<sup>e</sup>Referenece [87].

set removes the displacement. The A1 peak in ZnSe is not due to amorphous (a-) Se; the analogous peak in a-Se is 16 cm<sup>-1</sup> higher and a factor of 2 wider than in the ZnSe spectra [85,86].

In summary, both applied pressure and exposure to light are needed to produce the A1 and E'' peaks in <sup>68</sup>Zn <sup>76</sup>Se, signaling the precipitation of t-Se NCs within high-quality near-stoichiometric crystals. The thresholds of pressure and flux are ≥4.8 GPa and ≥50–70 W/mm<sup>2</sup>; heating is minimal since the light is sub-band-gap. The process does not reverse on decreasing pressure, and should not be mistaken for an anomalous phase change in the host, which continues to exhibit the same intrinsic phonons. The 4.8 GPa threshold is also well below the I-II phase transition in ZnSe at 13.0 GPa, so the A1 and E'' peaks cannot be associated with this transition either. Reappraisal of the pressure-Raman data for ZnM<sub>x</sub>Se<sub>1-x</sub> (M = Cd, Mn, Fe; 0 < x < 0.33) shows that t-Se NCs develop in these alloys at similar pressures of 4–5 GPa, evident again by appearance of the A1 peak [15–17,48,49].

### B. ZnTe

Te NCs can form in ZnTe under pressure and photon flux, as for Se in ZnSe. Similarly, the effect is signaled by growth of the t-Te A1 Raman peak [8]. The pressure range is lower, requiring closer study of the samples at 1 atm, and other aspects of the process are more complex. To clarify this, extensive experiments on <sup>64</sup>Zn<sup>nat</sup>Te bulk samples and on ZnTe MBE films were performed, and are reported in this section.

The Raman results at 1 atm in Fig. 4 explore how the tendency to form t-Te NCs depends on (i) cleaving of bulk samples, (ii) incident laser flux, and (iii) the BEP Zn:Te ratio for MBE films [88,89]. The uppermost spectrum in Fig. 4(a) is recorded on a large as-grown <sup>64</sup>Zn<sup>nat</sup>Te crystal using 647 nm light at the relatively high power of 600 mW (450 W/mm<sup>2</sup>). It shows only intrinsic features, as labeled [21,79]. There is no sign of the t-Te A1 mode, whose position at 1 atm is 123 cm<sup>-1</sup> [90,91]. The shoulder at 116 cm<sup>-1</sup> is due to the well-known ZnTe (TO-TA)(X) difference mode. The five lower spectra in Fig. 4(a) are measured on a razor-cleaved DAC chip of the same <sup>64</sup>Zn<sup>nat</sup>Te material using increasing 647 nm powers (60–240 mW). At the lowest power there is

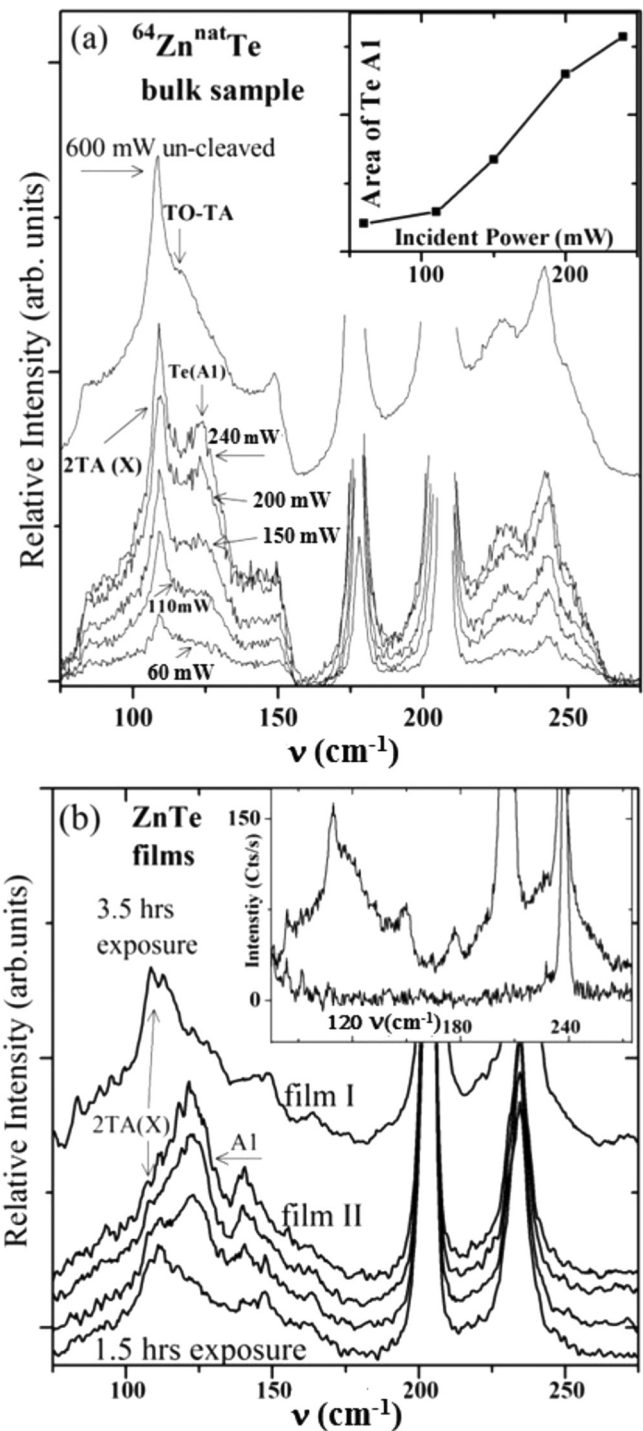


FIG. 4. Effects of laser power and sample preparation on ZnTe Raman spectra at 1 atm. (a) <sup>64</sup>Zn<sup>nat</sup>Te bulk material, measured on an un-cleaved sample and on a cleaved chip. Inset plots net area due to Te A1 peak vs power for the chip. (b) ZnTe MBE films grown using Zn-rich (film I) and Zn:Te equal (film II) BEPs. Film II spectra were recorded with four successive 20 min exposures. Inset compares spectra of film I and its GaSb substrate in a large sample.

little if any t-Te A1 signal. With increasing power this changes, and the Fig. 4(a) inset shows that rapid growth of the t-Te A1 peak occurs at ~100–200 mW (75–150 W/mm<sup>2</sup>). Since ZnTe is transparent to the 647 nm laser, it appears that growth of

the t-Te A1 peak in ZnTe is again *photon driven (or assisted)*, rather than caused by laser heating. Furthermore, the contrast between the results for the as-grown and cleaved samples indicates that *macroscopic defects enhance* the precipitation. In support of this, DAC chips cleaved by a sharp pin pressed at a *single point* (instead of razor cleaving along a *line*) are found to exhibit less tendency for the t-Te A1 peak to appear at 1 atm [92].

Figure 4(b) shows 1 atm Raman data for the two ZnTe/GaSb films listed in Table I. The uppermost spectrum, and the inset trace, are recorded on film I using high ( $440 \text{ W/mm}^2$ , 647 nm) and low ( $55 \text{ W/mm}^2$ , 568 nm) laser fluxes, respectively. Neither spectrum gives significant evidence of the t-Te A1 peak, even after 3.5 h of exposure in the former case. The four lower traces show how the 1 atm spectrum in film II evolves *with time* under high flux (again  $440 \text{ W/mm}^2$ , 647 nm). The t-Te A1 peak is initially absent in film II, but grows to roughly twice the height of 2TA(X) after 1.5 h. The different Zn:Te BEP ratios in these films leads to fewer  $V_{\text{Zn}}$  in film I than film II [60]. Hence, the Fig. 4(b) results suggest that a *higher density of  $V_{\text{Zn}}$  promotes* precipitation of t-Te NCs in ZnTe.

Initial pressure experiments on  $^{64}\text{Zn}^{\text{nat}}\text{Te}$  found that t-Te NCs precipitate with optimum efficiency below 0.9 GPa [8]. In Fig. 4(a) the tendency to form Te NCs at low pressure is found to be promoted by cleaving, suggesting that the stresses imposed by cleaving have an effect.

To define more clearly the optimum pressure for formation of t-Te NCs in bulk ZnTe, Raman experiments were carried out on  $^{64}\text{Zn}^{\text{nat}}\text{Te}$  for *decreasing* pressure. In each run, we first verify that the t-Te A1 peak is not detected in the cleaved DAC sample at 1 atm and very low flux ( $5 \text{ W/mm}^2$ , 647 nm). With the laser blocked, the pressure is raised to  $>5\text{--}6$  GPa, and spectra are recorded using the relatively high flux of  $175 \text{ W/mm}^2$  while reducing pressure. Figure 5 presents the results, comparing measurements in razor- and pin-cleaved samples at similar down-cycle pressures using three sub-band-gap laser lines. The t-Te A1 peak appears for  $P \lesssim 1.5$  GPa, and its strength tends to increase as the pressure is lowered further. Neither the laser wavelength, nor the cleaving method, strongly affects this general behavior. The optimum pressure range for the precipitation again tends to be below 1 GPa, similar to the initial estimate [8].

The Fig. 5 results seem counterintuitive, but the same trend occurs in repeated experiments. There is an *upper pressure* above which precipitation of t-Te NCs does not initiate. However, once the t-Te A1 peak appears, it remains on cycling the pressure above where the peak was absent initially. Hence, the precipitation is irreversible as found in ZnSe.

Of the two ZnTe MBE films, pressure-Raman data were recorded on film I, as summarized in Figs. 6(a) and 6(b). Because film I showed no detectable t-Te signal at 1 atm even for high laser flux [Fig. 4(b)], it could be studied under increasing pressure to explore the low-pressure onset of t-Te precipitation. This could not be done in film II. In these experiments, conducted at relatively low flux ( $55 \text{ W/mm}^2$ , 568 nm), the pressure is first raised from 0.2 to 3.2 GPa [Fig. 6(a)], then cycled down to 0.2 GPa, and up again to 5.4 GPa [Fig. 6(b)].

The t-Te A1 peak does not appear in the initial 0.2 GPa spectrum [Fig. 6(a), bottom trace]. The line shape is similar to

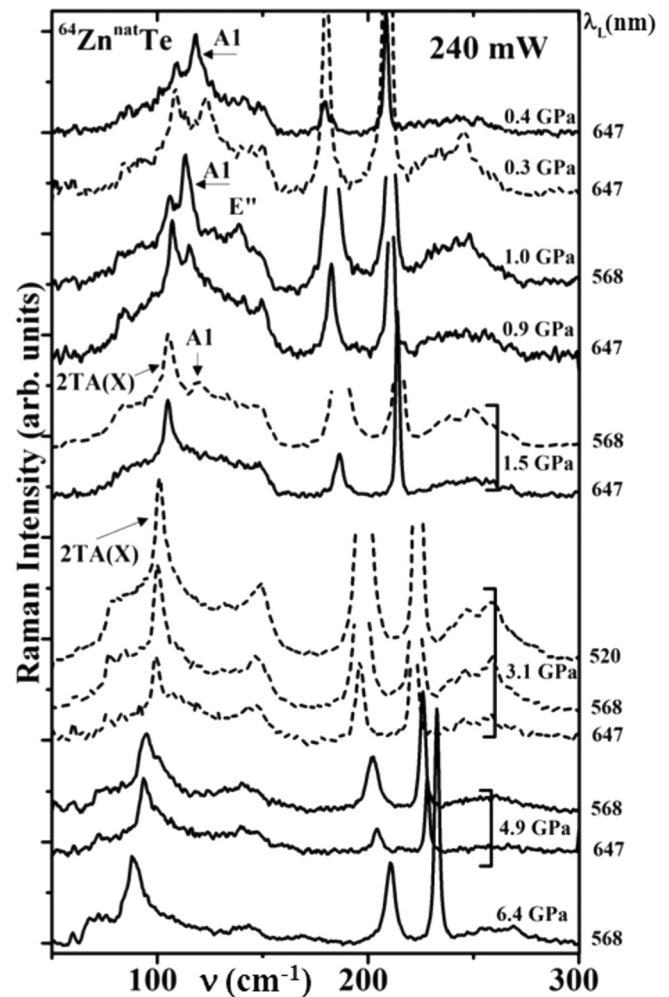


FIG. 5. Raman spectra of bulk  $^{64}\text{Zn}^{\text{nat}}\text{Te}$  recorded under decreasing pressure in separate samples using 520, 568, and 647 nm, as labeled at the figure's right edge. Solid (dashed) spectra are recorded on knife-cleaved (pin-cleaved) DAC chips.

that of the 1 atm result in the Fig. 4(b) inset, recorded on a large piece of the as-grown film using the same laser conditions. Again, note that the shoulder just above 2TA(X) derives from the *intrinsic* (TO-TA)(X) band [21]. A nonintrinsic feature slightly below the expected frequency of the t-Te A1 peak [81,90] enters the spectrum in the range 1.0–1.5 GPa. It is labeled A1<sub>-</sub> for reasons given below. On raising the pressure further to 3.2 GPa, this peak remains in the spectra, but we find that its strength levels off somewhere between 2.0 and 2.6 GPa.

On cycling down to 0.2 GPa, two nonintrinsic peaks now are observed at frequencies slightly above the positions of the A1 and E'' modes in t-Te crystals [81,90]. In Fig. 6(b) they are labeled A1<sub>+</sub> and E''. A1<sub>+</sub> has a strength comparable to LO( $\Gamma$ ) at 0.2 GPa, but intermediate scans show that A1<sub>+</sub> first appears strongly on decreasing pressure into the range 0.7–0.5 GPa. The dotted lines in Fig. 6(b) follow the shifts of A1<sub>+</sub>, E'', and 2TA(X) on the second pressure upstroke. At  $\sim 2.0$  GPa and above an additional nonintrinsic peak appears that again exhibits the frequency and pressure shift of A1<sub>-</sub>, and is dominant over A1<sub>+</sub> above 3.1 GPa. The film I experiments

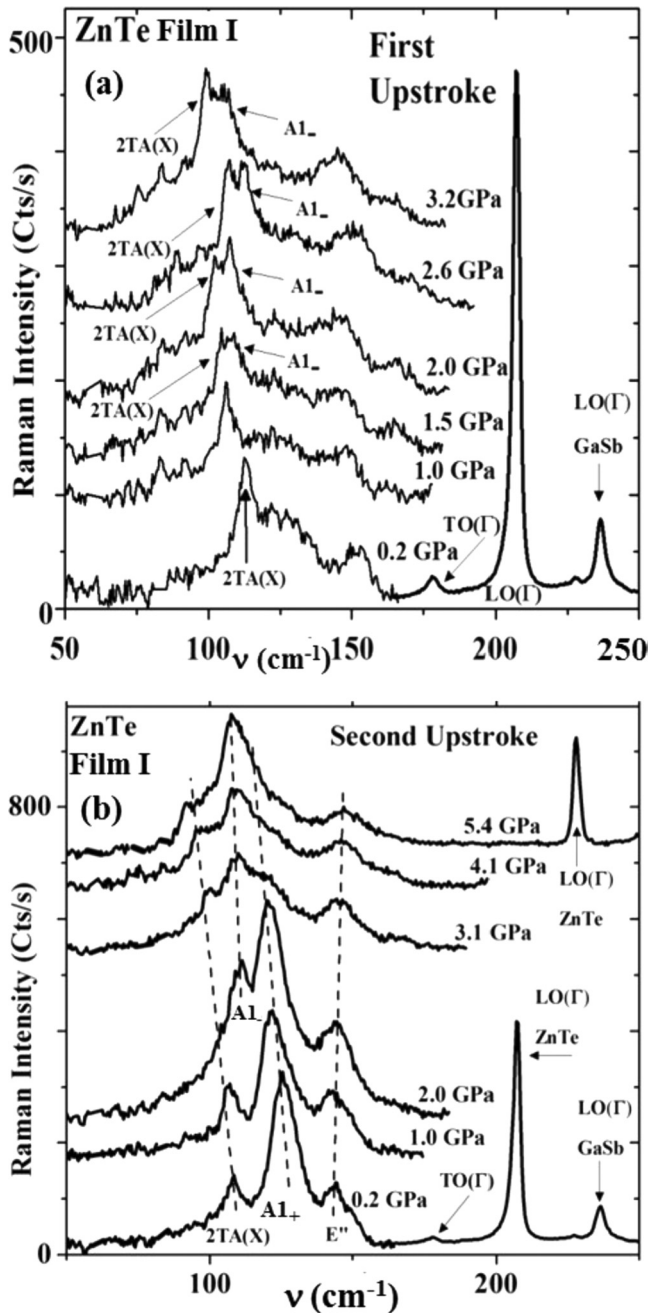


FIG. 6. Raman spectra of film I recorded using low 568 nm laser flux: (a) First cycle-up of pressure, and (b) second cycle-up of pressure. Peaks labeled  $A1_-$ ,  $A1_+$ , and  $E''$  are attributed to Te NCs. Dashed lines in (b) follow pressure shifts of these features and the intrinsic  $2TA(X)$  peak. The ZnTe  $2TA(L)$  shoulder, located  $\sim 28 \text{ cm}^{-1}$  below  $2TA(X)$ , is obscured by Raman scattering from air.

were repeated in an independent DAC loading, with rather similar results.

The pressure shifts of the Raman features in bulk  $^{64}\text{Zn}^{\text{nat}}\text{Te}$  and in film I are plotted in Figs. 7(a) and 7(b), respectively. The dashed curves give the best fit to the prior collective results for the  $A1$  mode in Te crystals [81,83–87] (Table II lists the fit parameters), and for the  $E''$  mode (nearly flat shift). The pressure behavior of the intrinsic modes in both  $^{64}\text{Zn}^{\text{nat}}\text{Te}$  and film I agree well with each other and with earlier

findings [1,6,93]. Likewise, in Fig. 7(a) there is good accord between the established results for the  $A1$  and  $E''$  modes in pure t-Te, and the pressure shifts of the analogous peaks in  $^{64}\text{Zn}^{\text{nat}}\text{Te}$ . The latter agreement (as for t-Se in ZnSe) is strong evidence that t-Te NCs have precipitated.

In Fig. 7(b) the frequencies and pressure shifts of the  $A1_+$  and  $A1_-$  peaks clearly differ from those of any ZnTe intrinsic modes. The pressure dependences of  $A1_+$  and  $A1_-$  appear to form two branches in the vicinity of the  $A1$  mode of t-Te (dashed curve). The  $A1_+$  data for  $P < 1.5 \text{ GPa}$  combined with the  $A1_-$  data for  $P > 1.5 \text{ GPa}$  approximately follow the t-Te  $A1$  mode.

Also the  $E''$  peak in film I has a slight upward shift instead of the virtually flat behavior of the analog peak in t-Te. The effects of pressure on the  $A1_+$ ,  $A1_-$ , and  $E''$  peaks in film I are more complex than found for the Te NC peaks in bulk  $^{64}\text{Zn}^{\text{nat}}\text{Te}$ . However, the nonintrinsic origin of  $A1_+$ ,  $A1_-$ , and  $E''$ , and their proximity to the  $A1$  and  $E''$  frequencies in pure t-Te for a wide range of pressures, lead us to again identify these peaks in film I with Te inclusions. We suspect that the differences between the bulk  $^{64}\text{Zn}^{\text{nat}}\text{Te}$  and film I results arise from the dual contributions in the film of Te inclusions formed close to, and away from, the substrate. The increased density and variety of defects near the film’s heterointerface, as well as the shear strain in this region, could well alter the structure and pressure response of the Te inclusions.

*Summary for ZnTe:* Our pressure-Raman results on ZnTe suggest that the precipitation of Te NCs is mediated by two effects—one that allows the NCs to nucleate, and a second that controls the growth rate of the NCs. The first effect depends on crystal quality such that Te NCs can begin to form at low pressure (even down to 1 atm), as found in the bulk samples damaged by razor cleaving or in the MBE film with higher vacancy content. However, in the vacancy-suppressed film I, the nucleation-onset effect requires between 1.0 and 1.5 GPa before Te NCs can appear. On the other hand, once the NCs are present, the second effect promotes a slower rate of growth at higher pressures. In fact, for pressures  $\gtrsim 1.5 \text{ GPa}$ , the NC growth is *suppressed below detection* in the down-cycle experiments on  $^{64}\text{Zn}^{\text{nat}}\text{Te}$  (Fig. 5). This upper limit is slightly higher,  $P \sim 2.0\text{--}2.6 \text{ GPa}$ , in film I, our best MBE material with low  $V_{\text{Zn}}$  content. For both the bulk and film samples, the optimum growth rate occurs below 1.0 GPa. We attribute effect one to the onset of plastic flow, and effect two to the probability for heterogeneous nucleation of NCs at dislocations. A model and calculations supporting this hypothesis is presented in Sec. IV.

### C. CdSe

Pressure-Raman experiments on the ZB CdSe film in Table I did not find strong evidence for precipitation of t-Se NCs. We summarize the results here as a counter case to ZnSe and ZnTe. For more details, see Ref. [8]. Previous measurements have been reported for the effects of pressure on the phonons and phase changes in bulk crystals of WZ CdSe and in colloidal nanoparticles of ZB CdSe [9,10].

The 1 atm Raman spectrum of our [001] CdSe film exhibits only the ZB-allowed  $\text{LO}(\Gamma)$  peak at  $208 \text{ cm}^{-1}$ , in accord with the prior 1 atm results on comparable films [71], and quite

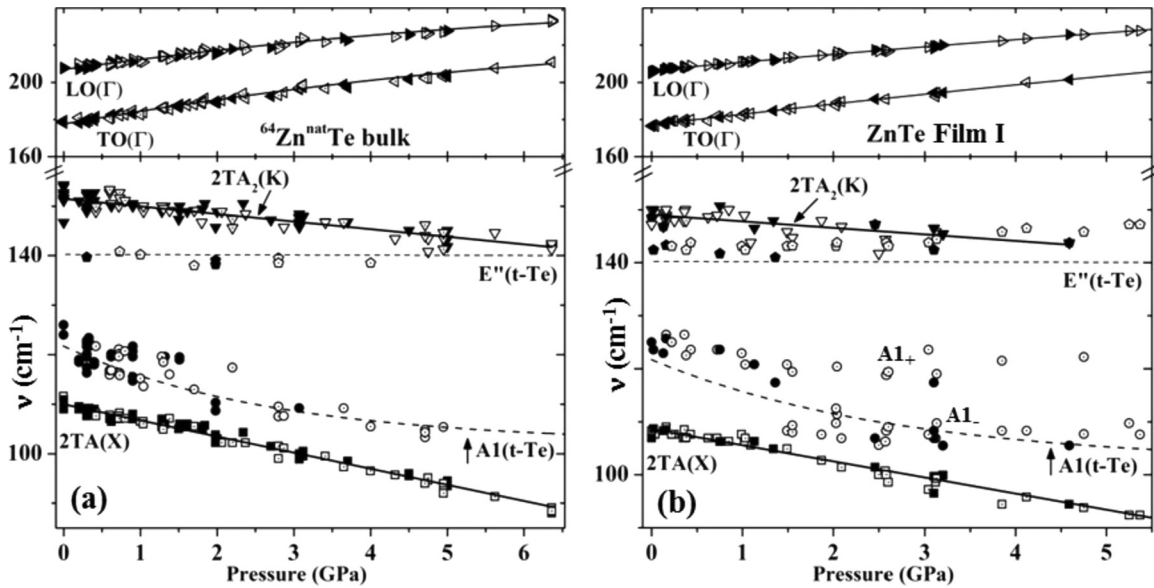


FIG. 7. Pressure shifts of intrinsic and Te-related Raman features in (a) bulk  $^{64}\text{Zn}^{\text{nat}}\text{Te}$ , and (b) MBE grown ZnTe in film I.  $A_1, A_{1+}, A_{1-}, E''$  arise from precipitated Te. Solid (open) symbols are our measured results for increasing (decreasing) pressure. Solid curves are best fits to these data. Dashed curves give the best-fit dependence of the  $A_1$  and  $E''$  modes in t-Te from compiled literature. (See text.)

close to the frequencies of the  $A_1(\text{LO})$  and  $E_1(\text{LO})$  peaks in WZ CdSe. The  $\text{LO}(\Gamma)$  peak in the ZB film shifts linearly with pressure at a rate of  $+4.6 \text{ cm}^{-1}/\text{GPa}$ , similar to the pressure shifts of the  $A_1(\text{LO})$  and  $E_1(\text{LO})$  peaks in WZ CdSe [9], and to the analogous peak in colloidal CdSe nanoparticles [10].

We observe a sharp decrease in the  $\text{LO}(\Gamma)$  intensity above 3.1 GPa, indicating that the I-II phase change is in progress. This pressure is higher than the 2.5 GPa transition in WZ CdSe (Table I) [45]. However, because the phase change is sluggish, the 0.6 GPa difference may not be meaningful. As for WZ CdSe, one expects phase II for ZB CdSe to have the NaCl structure, with no Raman active modes. In line with this, we find that the I-II transition of the ZB film is complete by 4.5 GPa, since for  $P > 4.5 \text{ GPa}$  only Raman features from the film's GaAs substrate are detected.

Between 3.1 and 4.5 GPa, three additional weak peaks appear near the CdSe  $\text{LO}(\Gamma)$  peak. These peaks have several possible origins. (i) They could arise from competing metastable CdSe phases—the cinnabar and WZ forms found in the transitions of other II-VI compounds are likely [6,38,39,93]. (ii) They could be due to material near the substrate that is partially transformed and subject to extra biaxial strain. (iii) Identification with the  $A_1$  peak of t-Se remains possible, since that peak also occurs in the *same frequency region* at these pressures.

Regarding the latter possibility, precipitation of Se NCs in CdSe should be an irreversible process, as for ZnSe and ZnTe. If the t-Se  $A_1$  peak had appeared in the range 3.1–4.5 GPa, it should be seen at other pressures. As noted, for  $P > 4.5 \text{ GPa}$  we detect only substrate Raman features. On decreasing the pressure (from 7 GPa) to reverse the I-II transition, multiple peaks again appear near  $\text{LO}(\Gamma)$ . However, for  $P < 1.5 \text{ GPa}$  we observe only a broadened (factor  $\sim 2.5$ )  $\text{LO}(\Gamma)$  peak that may indicate a mixture of ZB and WZ CdSe. There is no sign of the t-Se  $A_1$  peak, which would now appear over  $15 \text{ cm}^{-1}$  higher than the CdSe  $\text{LO}(\Gamma)$  position, and should be clearly resolved.

Hence, it is unlikely that Se NCs formed under pressure in the ZB CdSe film. This behavior is also explained by the model in Sec. IV.

#### IV. DISCUSSION

Precipitation effects are common in crystals subject to plastic deformation, as e.g., in tensile stress tests. Motion and multiplication of dislocations can result in partial decomposition (driven by vacancy chemistry) and nucleation of atomic species at dislocations and grain boundaries. See, e.g., Ref. [58]. However, plastic deformation is not ordinarily expected for hydrostatic compression of a binary cubic crystal, in which isotropic forces act simply to reduce the bond length. Nevertheless, a strong case can be made that the results in Sec. III stem from plastic deformation, and we develop this explanation here.

An initial hint that plasticity is involved comes from the observed pressure shifts of the Se and Te  $A_1$  peaks in bulk ZnSe and ZnTe. These shifts are the same as in pure t-Se and t-Te. Without plastic deformation, a cage effect, controlled by the compressibility of the host lattice, would tend to insulate the Se (Te) NCs from the full external pressure. This situation changes if dislocation motion creates a plastic region around the NCs. The plastic region serves as a pressure medium (like the DAC gasket fluid), able to reach mechanical equilibrium with the compressed host, and transmit the applied pressure to the NCs [94].

The two-stage model that we propose to explain our results is based on processes for precipitation hardening in metal alloys [58], as depicted in Fig. 8.

In stage one, local shear stresses that exceed the Peierls limit develop for sufficiently high hydrostatic pressure. Dislocations then move and multiply in the crystal, assisted by acoustic vibrations that arise from the defect photoexcitation processes discussed, under *Role of Light* below. In the tetrahedral

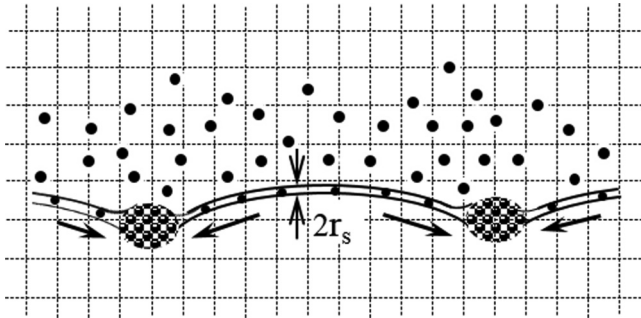


FIG. 8. Precipitation and growth of NC inclusions at sites on a vibrating dislocation line by heterogeneous nucleation of atoms captured from a surrounding Cottrell cloud made from crystal constituents.

semiconductors one typically finds  $60^\circ$  (hybrid edge-screw) dislocations, often dissociated into Schockley partial pairs with stacking faults in between [95,96]. Near the dislocation lines, strong lattice disruption can create Cottrell clouds of the host's atomic species, viz., concentrations of constituent atoms that tend to gather around the dislocation lines in randomly distributed positions. The motion and vibration of the dislocations allows them to sweep up atoms from the clouds. In ZnSe and ZnTe these clouds evidently are chalcogen rich. The Zn atoms are mobile [76,97], and most likely diffuse away toward the surface on a time scale comparable to that needed for the precipitate to form. This diffusion plays an important role in the process of chalcogen precipitation, as it precludes the cations from capture by the dislocations, reduces the coupling of the chalcogen anions to the cloud, and also preserves the stoichiometry in the undisturbed bulk of the host. In ZnSe, efficient photoinduced migration of Zn interstitials is observed even at cryogenic temperatures [97], and calculations indicate that the barriers for diffusion of Zn interstitials in the II-VIs can be strongly reduced (nearly to the point of spontaneous migration in ZnSe) depending on the excited Zn charge state [98].

In stage two, captured atoms move by rapid diffusion along the dislocations to nucleation sites, where heterogeneous growth of t-Se (t-Te) NCs becomes energetically favorable for nuclei larger than a minimum size. The rate of nucleation then controls the growth of precipitate inclusions. The theory is well understood due to the work of Cahn [57] and others [58]. In Appendix B we expand Cahn's treatment to include applied pressure.

There is an interesting connection of the present analysis to the mechanisms that degrade ZnSe-based blue lasers. Extensive work [99–101] suggests that, under the injection and light flux conditions of laser operation, dark-line defects related to dislocations in the active region and stacking fault decomposition are prime causes of laser failure. Although the context is different from the present work, we note that the processes proposed in stage one of the above model have similar driving mechanisms.

In the present work five questions should be addressed to explain our experimental results using the proposed two-stage model: (i) How does hydrostatic pressure cause plastic deformation? (ii) What is the role of light in this process?

(iii) How can we understand the different pressure ranges for chalcogenide precipitation in ZnSe and ZnTe—most puzzling is the existence of an upper pressure limit, as seen in ZnTe. (iv) To what extent can material preparation influence the tendency for plastic deformation and precipitation? (v) What accounts for the apparent lack of precipitation in CdSe?

#### A. Hydrostatic pressure and plastic deformation

Although the macroscopic average strain created by applied hydrostatic pressure in a cubic crystal is isotropic and homogeneous, local shear strains can arise due to a random distribution of defects that have noncubic site symmetry. Under hydrostatic pressure the strain field around, e.g., an axial defect, will reflect its symmetry and orientation. The interaction of the strain fields emanating from randomly oriented axial defects can then generate components of local shear strain that will increase with the applied pressure. Plastic flow commences when the corresponding shear stresses exceed the Peierls threshold  $\tau_p$  for motion of crystal dislocations. The simple picture gives [95]

$$\tau_p = \frac{2\mu}{1-\nu} \exp\left[\frac{-2\pi a}{b(1-\nu)}\right], \quad (1)$$

with  $\mu$  the shear modulus,  $\nu$  the Poisson's ratio,  $b$  the Burger's displacement, and  $a$  the lattice constant. It is more realistic to use estimates based on experiment. For the II-VI and III-V semiconductors one finds, respectively,  $\tau_p \sim 0.01\mu$  and  $\tau_p \sim 0.1\mu$  (see Ref. [95], Table 5.1). In ZnSe, ZnTe, and CdSe, this is only  $\sim 0.15$ – $0.35$  GPa, local shear stresses easily reached under the much greater applied pressures in our experiments. These are rough estimates. The observed shear stress needed for plastic flow also depends on crystal quality, temperature, and the methods of growth and sample preparation.

In the tetrahedral semiconductors one invariably finds axial defects. Typically they exhibit trigonal or tetragonal symmetry in their ground and/or excited states. The zinc vacancy  $V_{Zn}$  in ZnSe and ZnTe is a prime example. Studied in detail by Watkins and co-workers [76,102],  $V_{Zn}$  undergoes a tetrahedral-to-trigonal Jahn-Teller distortion that can be driven by sub-band-gap optical transitions between ground and excited states. Impurities paired with  $V_{Zn}$ , or paired with each other, at different neighbor separations exhibit similar distortions and give rise to manifolds of sub-band-gap energy levels. The Cu impurity is common in the Zn chalcogenides [73,74,103], and forms complexes of this type even in high quality material. (See Appendix A, Table IV, and references therein.)

#### B. Role of light

Under exposure to sub-band-gap light, the excitation and subsequent relaxation of such defects will generate acoustic phonons due to modulation of the distortions around the defect sites. The resulting shear waves can promote dislocation-line oscillations, and thereby the flow of dislocations by the usual glide and climb mechanisms [95]. We suggest that this contributes to the photoinduced precipitation effects observed in ZnSe and ZnTe. The cryogenic PL measurements on our ZnSe, ZnTe, and CdSe samples (see Appendix A) confirm the

presence of substantial concentrations (e.g.,  $10^{15}$ – $10^{18}$  cm $^{-3}$ ) of sub-band-gap axial defects. Since the rate of acoustic-energy loss to dislocations competes with other energy loss channels, it is reasonable that a threshold in light intensity will be needed to initiate sustained dislocation motion.

Another contributing factor may be photochemical reactions involving the bonding motifs of chalcogenide atoms, whose valence electrons support either the fourfold  $sp_3$  bonding of the host or the twofold  $sp_2$  chain bonding of Se and Te crystals. The  $sp_2$  bonding is known to be photosensitive because of the presence of nonbonding lone-pair electrons. Light may promote the nucleation of chalcogenide NCs at dislocations much as it promotes crystallization in amorphous Se [104,105].

At present it is not possible to determine which of these two photoassist mechanisms (or both) contributes to the observed precipitation of Se (Te) NCs under pressure in ZnSe and ZnTe.

### C. Low-pressure onset of precipitation and material preparation

ZnSe exhibits a sharp pressure threshold of  $P > 4.8$  GPa for formation of t-Se NCs. Similar results are found in  $\text{ZnM}_x\text{Se}_{1-x}$  ( $M = \text{Mn, Fe, Cd}$ ;  $0 < x < 0.33$ ) [13,15–18]. We interpret this threshold as the minimum applied pressure needed to induce the flow of dislocations. In ZnTe, the observed pressure threshold for t-Te precipitation is much lower and more dependent on crystal quality. Our best estimates put it at  $\sim 1.0$ – $1.5$  GPa in the ZnTe film with low  $V_{\text{Zn}}$  content. ZnTe is softer than ZnSe, and more prone to dislocations. ZnTe crystals often contain more as-grown defects than ZnSe, and high quality crystalline ZnTe tends to be more difficult to grow given the higher melting temperature of Te compared to Se [106]. Hence, it is not surprising that we observe photoinduced chalcogenide precipitation in ZnTe at a much lower pressure than in ZnSe, even occurring down to 1 atm in ZnTe chips subjected to high shear stress during cleaving, or in  $V_{\text{Zn}}$ -rich films.

### D. Cahn's model and high-pressure limit of NC precipitation

Harder to explain is the existence of an upper pressure limit for the NC precipitation, clearly shown by the down-cycle pressure results on ZnTe in Fig. 5. Within the context of Cahn's theory [57], (see Appendix B) we must consider the effects of pressure on the balance between the volume and surface terms in the energy of a NC nucleus decorating a dislocation, viz., the balance between the first and last two right-hand side terms in Eq. (B1). This controls the optimum shape and minimum size of the nucleus required to sustain NC growth without further activation. The energy barrier  $\mathcal{G}$  presented by this minimal nucleus depends on the parameter  $\alpha$  defined in Eq. (B2). Cahn's numerical solution for the variation of  $\mathcal{G}/\mathcal{G}_0$  vs  $\alpha$  ( $\mathcal{G}_0$  is the barrier against homogeneous nucleation) is reproduced in Fig. 12. In general, smaller  $\alpha$  leads to higher  $\mathcal{G}/\mathcal{G}_0$ . Pressure affects  $\alpha$  in two ways—through the  $Pf_v$  term in the Gibbs energy/volume gained on nucleation [Eq. (B3)], and through the pressure variation of the other factors in  $\alpha$ . The net fractional volume change  $f_v$  should be negative for condensation of NCs out of a Cottrell cloud,

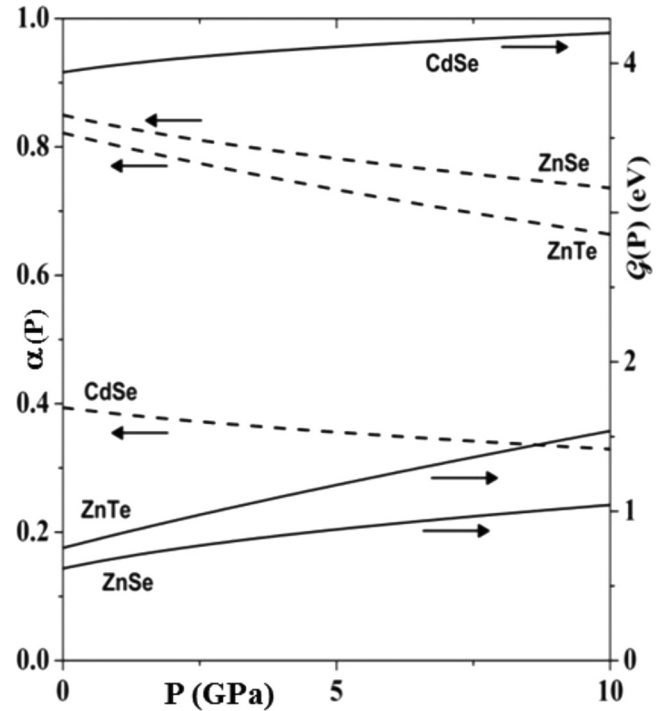


FIG. 9. Calculated pressure dependencies of the parameter  $\alpha(P)$  (dashed curves) and the energy barrier  $\mathcal{G}(P)$  (solid curves) for precipitation of Se or Te NCs at dislocations in ZnSe, ZnTe, and CdSe. See the text and Appendix B for details.

favoring enhanced precipitation at higher pressure. However, the pressure dependence of the other factors in  $\alpha$  tends to decrease its value. Hence, if  $f_v$  is not too large, a higher pressure can still act to inhibit precipitation.

To explore how this could work, we carry out calculations for ZnTe, ZnSe, and CdSe employing the modified Cahn theory. The calculations aim to fit our results by using as input approximate values of the barriers  $\mathcal{G}(P_{\pm})$ , deduced from experimental estimates of the precipitation density rates [Eq. (B4)] at the endpoints  $P_{\pm}$  of the pressure range where NCs form. Procedures for estimating  $\mathcal{G}(P_{\pm})$  and for doing the fits are given in Appendix B.

Figure 9 summarizes a set of illustrative results for  $\alpha(P)$  and  $\mathcal{G}(P)$ , and Table III lists the model parameters used to compute the plotted curves. Good fits to our results for ZnSe and ZnTe obtain for values of  $\alpha(0) \approx 0.80$ – $0.87$ , combined with net volume changes of  $f_v \sim -5\%$  to  $-15\%$ . One sees that  $\alpha(P)$  decreases with pressure. From Cahn's scaled plot (Fig. 11), this increases  $\mathcal{G}/\mathcal{G}_0$ , and that, in turn, increases the kinetic barrier  $\mathcal{G}$ . ( $\mathcal{G}_0$ , which contains the same volume and surface energies as  $\mathcal{G}$ , also grows with pressure.) In this way, higher pressures acts to turn off further growth of precipitate nuclei. The solid curves in Fig. 9 show the calculated increases in  $\mathcal{G}(P)$  with pressure for the materials studied here. The rise of the barrier in ZnTe is stronger than in ZnSe, as required by our results.

In doing these fits, we find that the  $P = 0$  values of the Helmholtz and surface energy-densities  $\Delta F$  and  $\gamma$ , respectively [Eqs. (B1) and (B3)], are sensitive to the choice of  $\alpha(0)$ . The  $\Delta F(0)$  and  $\gamma(0)$  values (Table III) used for the curves

TABLE III. Parameters used for Fig. 9 curves.

Parameter	ZnSe	ZnTe	CdSe
$\alpha(0)$	0.850	0.820	0.394
$\Delta F(0)(\text{eV}/\text{nm}^3)$	85.60	61.70	86.85
$\gamma(0)(\text{eV}/\text{nm}^2)$	16.14	13.00	16.42
$\mathcal{G}_0(\text{eV})$	9.610	9.630	9.834
$f_v$	-0.14	-0.05	-0.10
$\mu(\text{eV}/\text{nm}^3)$	205.63	155.00	85.00
$\nu$	0.35	0.35	0.35
$b(\text{nm})$	0.402	0.432	0.430
$\nu_\theta(\text{Hz})$	$7.1 \times 10^{12}$	$5.4 \times 10^{12}$	
$N_{\text{Se,Te}}(\text{cm}^{-3})$	$2.2 \times 10^{22}$	$1.98 \times 10^{22}$	
$L/2(\text{cm}^{-2})$	$10^9$	$10^9$	
$P_-(\text{GPa})$	4.8	0.0	
$P_+(\text{GPa})^a$	8.8	2.0	

<sup>a</sup>See note in Ref. [108].

in Fig. 9 should be regarded as upper limits. For both the precipitation of Se in ZnSe and Te in ZnTe, the  $\Delta F(0)$  are close to the cohesive energy density (CED) of t-Se and t-Te, respectively [107]; also, the  $\gamma(0)$  fall near  $\gamma(0) = r_{\text{at}}\Delta F(0)$ , where  $r_{\text{at}}$  is the average packing radius of atoms at 1 atm in t-Se or t-Te. Clearly smaller  $\Delta F(0)$  and  $\gamma(0)$  are possible depending on the binding of the Cottrell-cloud atoms to the host. The  $f_v$  parameters for the Zn compounds come out to be -14% and -5% for Se and Te precipitation, respectively. These values also are sensible, and similar to the volume decreases between the amorphous and trigonal forms of Se and Te [109].

### E. Absence of precipitation in CdSe

Because we observe no Se precipitation in CdSe, the plots in Fig. 9 for this material are calculated using the generic parameters  $\Delta F(0) \equiv (\text{CED of t-Se})$ ,  $\gamma(0) = r_{\text{at}}\Delta F(0)$ , and  $f_v = -10\%$ . We find that  $\alpha(P)$  is a factor of 2 smaller than for t-Se in ZnSe, a result caused by the softer shear modulus of CdSe [65]. The kinetic barrier  $\mathcal{G}(P)$  is then much higher (Fig. 9), and precipitation at room temperature is very improbable in CdSe. The choice of  $f_v$  does not strongly affect this outcome. To alter it, large changes in  $\Delta F(0)$  and  $\gamma(0)$  are needed. Thus, the present model supports the apparent lack of t-Se precipitation in CdSe. CdSe is an interesting case in which the low shear modulus favors dislocation formation, but works against nucleation of t-Se NCs.

Another factor that could inhibit t-Se precipitation in CdSe, in contrast to ZnSe, is inefficient Cd diffusion. The size difference of Cd and Zn may promote this. The covalent radius of Cd is 14% larger than the Zn radius, while the CdSe lattice constant is only 7% larger than in ZnSe. Also, although theory [98,110] suggests that photoinduced Cd diffusion should occur in the Cd-VI materials, the effect of photoexposure (reduction of the diffusion barrier) may be weaker than for Zn in ZnSe. However, one should keep in mind that besides atomic size and photoeffects, the densities of vacancies and other point defects, the polarity of the host and of charge trapped at dislocations, and rapid migration along grain boundaries can contribute to the diffusion [111]. Nevertheless, our calculated results for CdSe in Fig. 9 indicate

that, even for efficient Cd diffusion, the energy barrier against nucleation of t-Se NCs on dislocations in CdSe is too high to allow an appreciable precipitation rate at room temperature.

We have not carried out pressure-Raman experiments on CdTe as part of the present study. Te inclusions form readily during growth of bulk CdTe, as a result of the CdTe phase diagram [112,113]. Consequently, it would be problematic to distinguish between preexisting and newly precipitated Te in pressure experiments on CdTe like those reported here for ZnTe. Additional work, both experiment and theory, on pressure-induced precipitation effects in the Cd-chalcogenides is needed to clarify the behavior in these materials.

Although the calculated curves in Fig. 9, and the associated parameters in Table III, are not unique, the ranges of variation are limited. To illustrate: For Te NC precipitation in ZnTe, an acceptable fit also obtains for slightly higher  $\alpha(0)$ , e.g., taking  $\alpha(0) = 0.86$  ( $\sim 5\%$  larger), requires  $\Delta F(0) = 30.9 \text{ eV}/\text{nm}^3$ ,  $\gamma(0) = 8.99 \text{ eV}/\text{nm}^2$ , and  $f_v = -2.5\%$ , values appreciably smaller than before. This is still reasonable, and gives a viable homogeneous-nucleation barrier of  $\mathcal{G}_0(0) = 12.77 \text{ eV}$  (instead of 9.63 eV). However, for further increases in  $\alpha(0)$ , one quickly enters an unstable regime in which  $\mathcal{G}/\mathcal{G}_0$  gets very small (see Fig. 12). Indeed, for  $\alpha > 1$ , the dislocations become unstable along their entire length [58]. Massive damage would result even at  $P = 0$ , clearly not the case for the crystals in our study. Likewise, smaller values of  $\alpha(0)$  are problematic, since they yield unrealistic large values of  $\Delta F$ , greater than the CED of Te. Taking  $\alpha(0) = 0.78$  ( $\sim 5\%$  smaller), requires  $\Delta F(0) = 118.9 \text{ eV}/\text{nm}^3$  ( $\sim 2 \times \text{CED}$ ),  $\gamma(0) = 18.53 \text{ eV}/\text{nm}^2$ ,  $f_v = -10\%$ , and  $\mathcal{G}_0(0) = 7.53 \text{ eV}$ .

The energy densities  $\Delta F(0)$  and  $\gamma(0)$  that mediate the NC nucleation are very difficult to compute. Atomic cluster calculations combined with Monte Carlo simulations of the nucleation process may offer more accuracy and microscopic insight than the Cahn model, and should be pursued. However, the present analysis provides a reasonable explanation for the tendencies of chalcogenide atoms to form NC precipitates under applied pressure and photoexcitation in ZnSe and ZnTe, as well as for the absence of NC precipitation in CdSe. We believe that this treatment captures the physics of these complicated effects.

## V. IMPLICATIONS FOR HIGH-PRESSURE PHASE TRANSFORMATIONS

Plastic deformation and NC precipitation create structural and chemical disorder. If one or both of these disorders occur at pressures below a crystal's I-II transition, what will be the effects on the transition and its observation?

Pressure-induced plastic deformation is an issue for the I-II phase change when the pressure needed to generate local shear stresses above the experimental  $\tau_p$  is below the transition threshold  $P_{\text{I-II}}$ . Soft crystals with low shear moduli but relatively high  $P_{\text{I-II}}$  are susceptible, especially if there is a high density of low-symmetry defects. ZnSe and ZnTe are good candidates, and probably also CdSe due to its softness even though its  $P_{\text{I-II}}$  is low.

However, during the I-II transitions in semiconductors, dislocations and grain boundaries invariably form and influence

the phase change as discussed by Besson *et al.* [47]. We expect that the situation will not be considerably altered in crystals subject to low-pressure plastic deformation *without precipitation*. The transition should be similar, with little effect on the observed forward and reverse thresholds, the kinetics, and the progression of local structural changes.

In contrast, the chemical disorder caused by NC precipitation in phase I is problematic for observing the I-II transition. In x-ray, Raman, or other experiments, when new data features are interpreted as phase changes, questions arise as to which changes in which parts of the crystal? The new features may be due to the host's I-II transition, or may signal NC formation as in ZnSe and ZnTe. With further increase of pressure, the NCs may undergo separate phase changes that likewise could be misinterpreted. The new features might also arise from host regions that are enriched in anions or cations, but not fully segregated. The phase transitions in such regions will depend on their compositions, and could lead to confusion. For instance, the forward-reverse transition hysteresis will be broadened, and changes seen in this pressure range are vulnerable to misidentification. This may account for some of the complex phases observed in ZnSe and ZnTe during their reverse II-I transitions (e.g., mixtures of distorted wurtzite, cinnabar, and/or NaCl structures) [6,45,48,93]. The possibilities for confusion in pressure studies of alloys [13,15–18,49] should be even stronger.

We propose a test to judge the susceptibility of materials to NC precipitation under hydrostatic pressure. Elemental crystals, of course, are not subject to chemical inhomogeneity. For compound crystals the test requires two parameters. First, the likelihood that plastic deformation will occur for  $P < P_{I-II}$  is gauged by the ratio  $P_{I-II}/\tau_p$ . The higher this ratio, the greater is the chance for plasticity in phase I. Second, the probability to nucleate NCs on dislocations is gauged by the parameter  $\alpha(P=0)$  in Cahn's model [57]. At room temperature, this probability should be relatively high for  $0.75 \leq \alpha < 1$ , appreciably lower for  $0.60 \leq \alpha < 0.75$ , and very unlikely for  $\alpha < 0.60$ . For higher temperatures, these ranges extend to lower  $\alpha$ .

In Fig. 10 this test is applied for precipitation of anion NCs in several common semiconductors. To estimate  $\alpha(0)$ , one needs the  $P=0$  values of  $\mu$  and  $b$  for the hosts and  $\Delta F$  and  $\gamma$  for the precipitates [Eqs. (B1)–(B3)]. In these materials  $b \approx a/\sqrt{2}$  [95],  $\mu$  is well known [65,114], and from our prior discussion, a lower limit of  $\alpha(0)$  is obtained by using the anion's CED [107] for  $\Delta F$  and taking  $\gamma = r_{at}\Delta F$ . Also we take  $\tau_p = 0.01\mu$  ( $0.1\mu$ ) for the II-VI (III-V) compounds as per the experimental estimates in Ref. [95] (Table 5.1), and for  $P_{I-II}$  the values in Ref. [45] are used. (A similar test for the cation NCs is possible [115].)

Figure 10 predicts the following: ZnSe and ZnTe fall within the region of high probability for NC precipitation in phase I (upper right). CdSe (also CdTe and CdS) are susceptible to plastic deformation for  $P < P_{I-II}$ , but not to NC nucleation because  $\alpha$  is small. These predictions agree with our experiments. ZnS appears to be an intermediate case. The III-V materials are more resistant to plasticity, so single crystals are unlikely to exhibit NC formation in phase I under applied pressure. However, for finely powdered III-V samples, where high dislocation densities are introduced, the Ga-V and Al-V

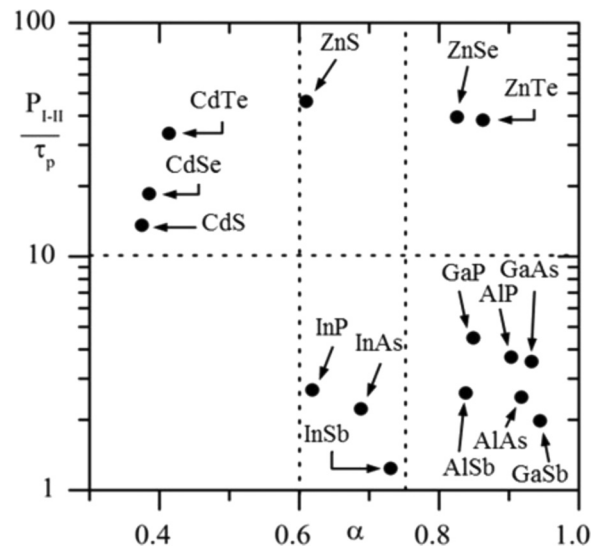


FIG. 10. Map proposed to predict the tendency for precipitation of anion NCs in common binary semiconductors at pressures below  $P_{I-II}$ . (See text.)

series with large  $\alpha$  are vulnerable, and the In compounds lie in the middle range. For these III-V materials, discrepancies may then be expected between pressure experiments on powders and single crystals—due to precipitation effects in the former, absent in the latter. This is most likely to show up along the transition path, where the sequence of *local* structure changes may depend more on the chemical inhomogeneity than on the host crystal. To resolve these issues, future studies should systematically compare the pretransition disorder in powder and crystal samples. The map in Fig. 10 can serve as a guide for those challenging experiments.

## VI. SUMMARY AND CONCLUSIONS

Pressure-Raman experiments show that, under applied hydrostatic pressure and exposure to sub-band-gap light, chalcogenide NCs can be made to precipitate in high-quality closely stoichiometric II-VI crystals. The effect is demonstrated in ZnSe and ZnTe, but probably does not occur in CdSe. The NCs are detected in Raman spectra by the appearance of the A1 breathing-mode peaks of t-Se and t-Te, and the negative pressure shifts of those peaks. These shifts are not modified by the compressibility of the host lattice, but are the same as in bulk crystals of Se and Te. For ZnSe, the onset pressure and light threshold for t-Se NCs to form are  $\sim 4.8$  GPa and  $50\text{--}70$  W/mm<sup>2</sup>. For ZnTe, t-Te NCs are observed to nucleate at pressures  $\lesssim 1.5$  GPa in cleaved bulk samples, but this upper limit appears to be shifted slightly higher to  $\sim 2.0\text{--}2.6$  GPa in a MBE film with low  $V_{Zn}$  content. ZnTe films with more  $V_{Zn}$  defects, and bulk samples with strong cleavage damage, show greater tendencies for t-Te NCs to form at lower flux levels (typically  $\sim 75\text{--}150$  W/mm<sup>2</sup>) and lower pressures (even down to 1 atm). However, in our low  $V_{Zn}$ -content MBE film, Te precipitation does not onset until the pressure increases to  $\sim 1.0\text{--}1.5$  GPa. These sample trends, and the unimportance of the host compressibility for the pressure shifts of the NC peaks, offer strong evidence that plastic flow is involved.

We conclude that a two-stage mechanism is operative. (i) Hydrostatic-pressure-induced plastic deformation creates dislocations and grain boundaries that provide sites for NCs to condense. (ii) Se (Te) atoms released by the disrupted lattice condense into NCs at these sites. In this stage, the growth rates of the Se (Te) NCs are limited by the kinetic barriers to nucleation. Applied pressure acts to produce the plastic flow by increasing the internal shear forces around axial defects, eventually surpassing the Peierls limit. We expect that  $V_{Zn}$  centers and Cu complexes participate; their presence in our samples is confirmed by PL measurements. The axial distortions of these defects are photoactive, providing a plausible mechanism for light to assist the plastic flow and precipitation *via* fluctuations in the internal shear fields.

This mechanism is supported by calculations of the kinetic barriers for growth of Se (Te) NCs on dislocations. Our treatment employs Cahn's theory, modified to include pressure. The calculated kinetic barriers are able to fit experimental estimates of the NC nucleation rates using reasonable input parameters related to the cohesive energy densities of Se and Te. The results confirm that higher pressure can turn off the precipitation by increasing the nucleation barrier. We also find that the barrier in CdSe is too large to allow significant precipitation at room temperature. Hence, the proposed mechanism explains the major puzzling results in our experiments.

Based on these ideas, a scheme is developed to predict whether similar pressure-induced NC precipitation is likely in other binary semiconductors at pressures below the I-II phase change. If this occurs, the resulting chemical inhomogeneity can confuse observations of the transition. Powdered samples are especially vulnerable because of their high dislocation density.

**ACKNOWLEDGMENTS**

The authors are indebted to M. Cardona and J. K. Furdyna for a number of insightful discussions, and for generously providing samples for this work. We are grateful to R. Lauck and X. Liu for growth of the bulk and film samples, respectively, to Nelson Gross for providing help with the numerical analysis, and Dante Iozzo for assisting with the photoluminescence characterization. G.P.L. acknowledges support during this work from the SUNY at Buffalo Physics Department.

**APPENDIX A**

Figures 11(a)–11(d) show the PL spectra at 1 atm and 13 K of the ZnSe, ZnTe, and CdSe samples in this work; assignments of the labeled features are made based on the cited reports in Table IV. We do not attempt to identify all of the defects in our samples. Donors such as  $Al_{Zn}$ ,  $Ga_{Zn}$ ,  $Cl_{Se(Te)}$ , acceptors such as  $Li_{Zn}$ ,  $Na_{Zn}$ ,  $As_{Se(Te)}$ , and amphoteric O are all common, as are the defects  $V_{Zn}$  and  $Cu_{Zn(I)}$ , noted in the text, that give rise to axial centers [74,76].

The bulk  $^{68}Zn^{76}Se$  and  $^{64}Zn^{nat}Te$  spectra [Figs. 11(a) and 11(b)] exhibit prominent sharp PL lines at the customary energies assigned to the donor-bound excitons and the (somewhat deeper) acceptor-bound excitons in these materials [73,103,116,117]. LO phonon replica of several of these lines are also seen in both samples. The weak  $Y_0$  line

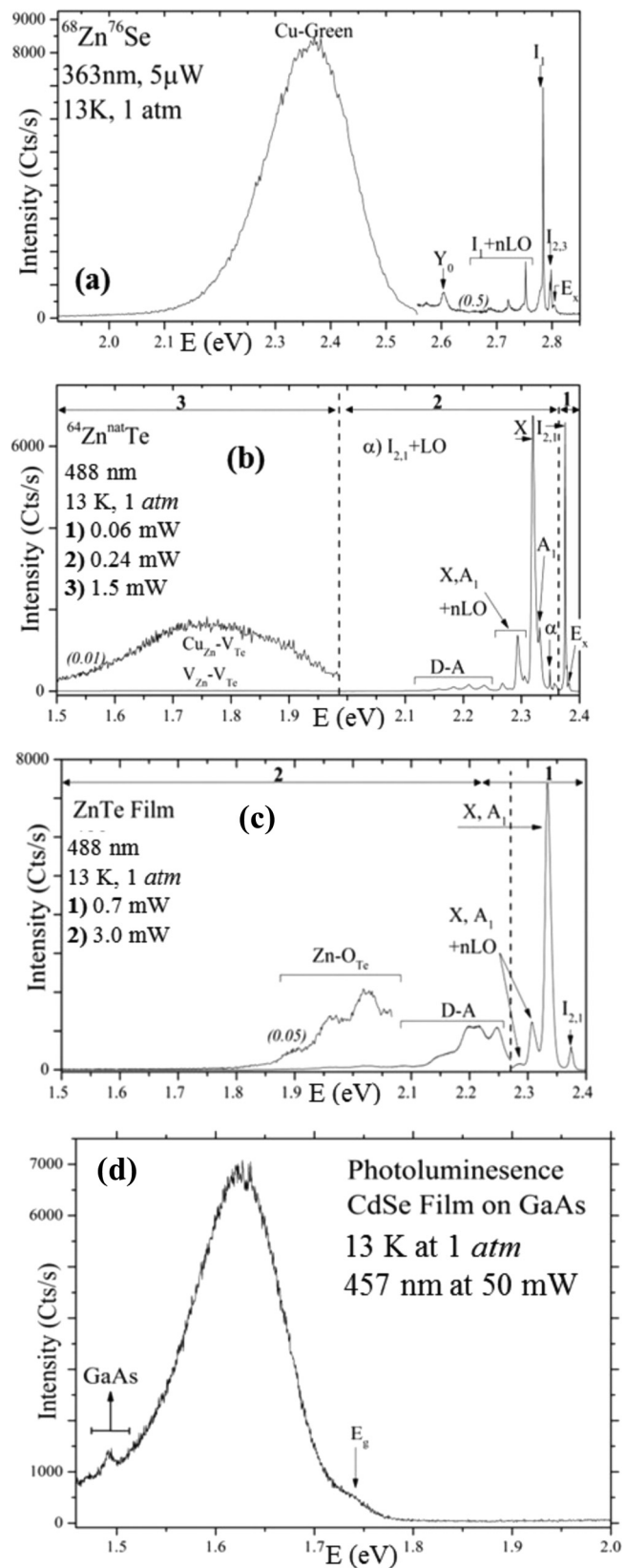


FIG. 11. PL spectra at 1 atm and 13 K characterizing the (a) ZnSe, (b) and (c) ZnTe, and (d) CdSe samples investigated in this work. The data in (c) is for film I.

TABLE IV. PL assignments in present samples.

Peak	$E$ (eV) exp.	$^{68}\text{Zn } ^{76}\text{Se}$ bulk sample peak assignments
$E_x$	2.804	free exciton <sup>a,b</sup>
$I_2(I_3)$	2.799 (2.796)	excitons bound to neutral <sup>a,b</sup> (ionized <sup>a</sup> ) shallow donors
$I_1(I'_1)$	2.784 (2.778)	excitons bound to $\text{Cu}_{\text{Zn}}(\text{V}_{\text{Zn}})$ deep neutral acceptors <sup>a,b,c,d</sup>
$I_1 + n\text{LO}$	2.752–2.685	phonon replicas of $I_1$ <sup>a,b,c,d</sup>
$Y_0$	2.604	excitons at dislocations <sup>a,e</sup>
Cu-green	2.370 (max)	shallow donor to $[\text{Cu}_{\text{Zn}}\text{-Cu}_I]$ deep acceptor complex <sup>f,g</sup>
Peak	$E$ (eV) exp.	$^{64}\text{Zn}^{\text{nat}}\text{Te}$ bulk sample peak assignments
$E_x$	2.381	free exciton <sup>h,i,j</sup>
$I_2(I_1)$	2.378 (2.375)	excitons bound to neutral shallow donors (acceptors) <sup>h,i,j</sup>
$A_1(X)$	2.331 (2.320)	free $\rightarrow$ bound to 1 <sup>st</sup> acceptor ioniz. level of $\text{V}_{\text{Zn}}$ ( $\text{Cu}_{\text{Zn}}$ , or other acceptors) <sup>h,i,k</sup>
$A_1(X) + n\text{LO}$	2.306–2.276	LO phonon replica of $A_1(X)$ <sup>h,i,k</sup>
$B$ series	2.236–2.157	free $\rightarrow$ bound to 2 <sup>nd</sup> acceptor ioniz. level of $\text{V}_{\text{Zn}}$ or $\text{Cu}_{\text{Zn}}$ , and $n\text{LO}$ replica <sup>h,i,k</sup>
Red band	1.75 (max)	shallow donor to deep acceptor complex, e.g., $[\text{Cu}_{\text{Zn}}\text{-V}_{\text{Te}}]$ , or $[\text{V}_{\text{Zn}}\text{-D}]$ , etc. <sup>h,k,l</sup>
Peak	$E$ (eV) exp.	ZnTe film I sample peak assignments
$I_2(I_1)$	2.376 (2.374)	excitons bound to neutral shallow donors (acceptors) <sup>h,i,j</sup>
$A_1(X)$	2.310	free $\rightarrow$ bound to 1 <sup>st</sup> acceptor ioniz. level of $\text{V}_{\text{Zn}}$ ( $\text{Cu}_{\text{Zn}}$ , or other acceptors) <sup>h,i,j</sup>
$A_1(X) + n\text{LO}$	2.30–2.27	LO phonon replica of $A_1(X)$ <sup>h,i,j</sup>
$B$ series + DAP	2.27–2.08	free $\rightarrow$ bound to 2 <sup>nd</sup> acceptor ioniz. level of $\text{V}_{\text{Zn}}$ or $\text{Cu}_{\text{Zn}} + n\text{LO}$ <sup>h,i,j</sup> + donor-accept. pair PL <sup>m</sup>
O-center PL	2.05–1.80	shallow donor to $[\text{Zn-O}_{\text{Te}}]$ deep acceptor complex <sup>j,k,m</sup>

<sup>a</sup>Reference [73].

<sup>b</sup>Reference [124].

<sup>c</sup>Reference [125].

<sup>d</sup>Reference [126].

<sup>e</sup>Reference [127].

<sup>f</sup>Reference [74].

<sup>g</sup>Reference [128].

<sup>h</sup>Reference [103].

<sup>i</sup>Reference [116].

<sup>j</sup>Reference [117].

<sup>k</sup>Reference [119].

<sup>l</sup>Reference [129].

<sup>m</sup>Reference [130].

in Fig. 11(a) indicates that the  $^{68}\text{Zn } ^{76}\text{Se}$  sample contains a residual density of extended defects. In the  $^{64}\text{Zn}^{\text{nat}}\text{Te}$  data, the series of donor-acceptor (D-A) peaks (and their LO replica) at 2.1–2.25 eV are attributed to transitions between shallow donor levels and the deep second-ionization state of  $\text{V}_{\text{Zn}}$  (a double acceptor).

The broad low-energy bands in Figs. 11(a) and 11(b) arise from strongly lattice-relaxed axial PL centers that, in cubic crystals, generally have trigonal or tetragonal site symmetry. The  $^{68}\text{Zn } ^{76}\text{Se}$  spectrum exhibits intense Cu-green PL (2.1–2.5 eV) that is identified with transitions between shallow donors and axial  $[\text{Cu}_{\text{Zn}}\text{-Cu}_I]$  deep acceptor complexes [74]. For  $^{64}\text{Zn}^{\text{nat}}\text{Te}$ , the band at 1.6–1.9 eV is attributed to exciton recombination at axial centers arising from  $\text{Cu}_{\text{Zn}}\text{-V}_{\text{Te}}$  or  $\text{V}_{\text{Zn}}\text{-V}_{\text{Te}}$  pairs. The weakness of this band suggests that the density of Te vacancies is low in the  $^{64}\text{Zn}^{\text{nat}}\text{Te}$  sample [118].

The spectrum of the ZnTe MBE film I sample [Fig. 11(c)] exhibits bound-exciton lines (2.28–2.40 eV) and a D-A series (2.08–2.27 eV) similar to those in the  $^{64}\text{Zn}^{\text{nat}}\text{Te}$  bulk crystal. However, the film's features are broadened, and the exciton

lines are  $\sim 13$  meV higher in energy, indicating some residual disorder and compressive strain from the interfacial region. The other assignments are also similar to the bulk sample, except that in the film diffusion from the GaSb substrate should increase  $\text{Ga}_{\text{Zn}}$ , and may introduce  $\text{Sb}_{\text{Te}}$  deep acceptors. The latter may enhance the broadening in the D-A series (2.08–2.27 eV), as proposed for  $\text{As}_{\text{Te}}$  in ZnTe films on GaAs [117].

Unlike the bulk  $^{64}\text{Zn}^{\text{nat}}\text{Te}$  sample, the ZnTe MBE film I sample does not have a band at 1.6–1.9 eV due to  $\text{Cu}_{\text{Zn}}\text{-V}_{\text{Te}}$  or  $\text{V}_{\text{Zn}}\text{-V}_{\text{Te}}$  pairs. This reflects the high purity and the Zn-stabilized conditions of the film I MBE growth. However, the film has another D-A series that is very weak at 1.9–2.1 eV. Its origin may be residual Zn-O acceptors, which also should be axially distorted [119].

The PL spectrum of the CdSe film [Fig. 11(d)] exhibits a broad intense peak at 1.63 eV, with a shoulder at 1.73 eV due to near-band-edge transitions. The band gap of ZB CdSe at this temperature is 1.75 eV, about 0.08 eV below the band gap of WZ CdSe [61,71]. In WZ CdSe, D-A transitions (and their LO replica) often lead to strong overlapping PL bands at energies

of 1.67–1.74 eV [120–123]. Assuming the D-A PL shifts with the band gap by the same  $-0.08$  eV, it is reasonable to assign the 1.63 eV peak in Fig. 11(d) to similar D-A transitions.  $\text{Li}_{\text{Cd}}$  and  $\text{Na}_{\text{Cd}}$  are common acceptors in CdSe, and the same alkali atoms as the interstitials  $\text{Li}_i$  and  $\text{Na}_i$  typically serve as donors.  $\text{Ga}_{\text{Cd}}$  donors and  $\text{As}_{\text{Se}}$  acceptors are expected as well because of the film's GaAs substrate. Also in CdSe, isolated  $\text{V}_{\text{Se}}$  and  $[\text{V}_{\text{Se}}\text{-acceptor}]$  pairs are important double and single donors, respectively, that could contribute to the 1.63 eV band [120]. The lack of structure and large width of this band suggest strong disorder even though the crystal quality away from the substrate (where the PL is emitted) is excellent. We suspect that electric-field fluctuations due to trapped space-charge near the substrate is a major source of this disorder [95].

### APPENDIX B

Cahn's theory [57] considers the Gibbs free energy per unit length  $\Gamma$  of a dislocation line decorated with precipitate and expanded to a cylinder radius  $r$ . We have

$$\Gamma = 2\pi\gamma r - \frac{b^2\mu}{4\pi(1-\nu)} \ln\left(\frac{r}{r_0}\right) - \pi r^2 \Delta G. \quad (\text{B1})$$

Here  $\Delta G$  is the gain in Gibbs free energy/volume on precipitation ( $\Delta G > 0$  by definition),  $\gamma$  (also  $> 0$ ) is the interfacial energy/area between precipitate and host,  $r_0$  is the dislocation core radius,  $b$  is the Burger's displacement,  $\mu$  is the shear modulus of the host, and  $\nu$  its Poisson ratio. Stable cylindrical dislocations exist when  $\Delta G < \Delta G_c$  or, using the parameter  $\alpha \equiv \Delta G/\Delta G_c$ , when

$$\alpha = \frac{b^2\mu\Delta G}{2\pi^2\gamma^2} < 1. \quad (\text{B2})$$

The stable cylinder radius  $r_s$  depends on  $\alpha$ . However, for a given  $\alpha < 1$ , further precipitation on the dislocation in a local bulge that exceeds a minimum size can still be energetically favorable. Solving for the shape of the bulge that minimizes the excess free energy relative to a stable cylinder of uniform radius  $r_s$ , one obtains the energy barrier  $\mathcal{G}$  for further growth of the bulge with steadily decreasing free energy. The solution is given conveniently in terms of a scaled plot of  $\mathcal{G}/\mathcal{G}_0$  vs  $\alpha$  [57], where  $\mathcal{G}_0 = \frac{16\pi\gamma^3}{3(\Delta G)^2}$  is the energy barrier for homogeneous nucleation. This plot is reproduced in Fig. 12.

We introduce the applied hydrostatic pressure  $P$  as follows. For a given constant  $P$ ,

$$\Delta G = \Delta F - P \frac{\Delta V}{V} = \Delta F - P f_v, \quad (\text{B3})$$

where  $\Delta F$  is the Helmholtz energy density gained on precipitation of t-Se (t-Te) out of the Cottrell cloud at temperature  $T$ , and  $f_v$  is the associated net fractional volume change. The energy densities  $\Delta F$  and  $\gamma$  should be scaled, respectively, by  $V(0)/V(P)$  and by  $[V(0)/V(P)]^{2/3}$ ; to do this we use the measured equations of state for Se (Te) [131,132]. We also scale  $b$  using the equations of state for ZnSe (ZnTe) [38], and we neglect the  $P$  dependence of  $\mu$  as a higher order

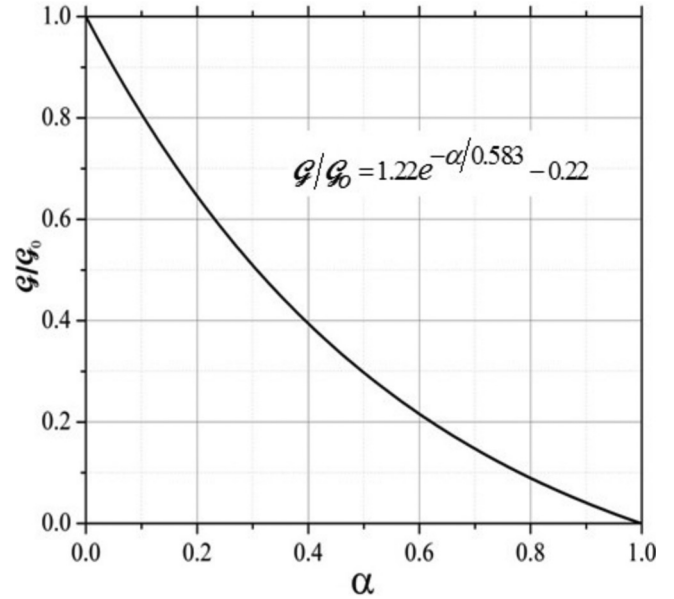


FIG. 12. Solution for the energy barrier  $\mathcal{G}$  (in units of  $\mathcal{G}_0$ ) vs  $\alpha$ . See Appendix B text. Curve after Ref [57]. Inserted equation is close fit found in the present work.

effect. Hence, given  $f_v$  and values for  $\Delta G(0) \equiv \Delta F(0)$  and  $\gamma(0)$  at 1 atm,  $\alpha$  can be obtained as a function of  $P$ , and the energy barriers  $\mathcal{G}(P)$  and  $\mathcal{G}_0(P)$  found from the plot in Fig. 12 and the expression for  $\mathcal{G}_0$ .

To test this model, a converse analysis is employed. We first estimate  $\mathcal{G}(P)$  at  $P_-$  and  $P_+$ , the endpoints of the active NC precipitation range. These estimates are derived from the observed precipitation-density-rates  $N_D$  for the chalcogenide NCs. One has [57]

$$N_D \approx \nu_\theta (N_{\text{Se,Te}})^{1/3} L \exp\left(-\frac{\mathcal{G}(P)}{kT}\right), \quad (\text{B4})$$

where  $\nu_\theta$  is the Debye frequency,  $N_{\text{Se,Te}}$  is the density of Se or Te atoms in the host crystal, and  $L$  is the total length of dislocations per unit volume (twice the areal dislocation density). To carry out the calculations we adopt  $\frac{L}{2} = 10^9 \text{ cm}^{-2}$  as a reasonable value in line with the high dislocation densities expected to form under the large DAC pressures. [For given  $N_D$ , a factor  $\xi$  decrease in  $L$  reduces  $\mathcal{G}(P)$  by  $-kT \ln \xi$ , not a strong effect.] The estimated  $\mathcal{G}(P_\pm)$  are then combined with different choices of  $\alpha(P=0)$  in order to explore whether realistic results for  $\Delta F$ ,  $\gamma$ , and  $f_v$  can be obtained while still fitting the main features of our experiments.

Based on the strength of the Se and Te A1 Raman peaks, and the noise in the Raman spectra, our detection criterion is a density of t-Se or t-Te that is  $\sim 10^{-3} \times$  (host density)  $\sim 10^{19} \text{ cm}^{-3}$ . Then given the observed time periods,  $\sim 2000$  s in ZnSe and  $\sim 200$  s in ZnTe, needed to detect NC formation at the pressures of its onset, we take  $N_D(\text{Se}) \sim 5 \times 10^{15} \text{ cm}^{-3}/\text{s}$  and  $N_D(\text{Te}) \sim 5 \times 10^{16} \text{ cm}^{-3}/\text{s}$ . Furthermore, for the practical turn-off limit for observing active NC formation we adopt  $N_D(\text{Se,Te}) \sim 5 \times 10^{13} \text{ cm}^{-3}/\text{s}$ , since at that rate it would take over two days to nucleate  $10^{19} \text{ cm}^{-3}$  NC atoms. In this way we establish  $\mathcal{G}(P_-)$  and  $\mathcal{G}(P_+)$  for ZnSe and ZnTe. Using

these barrier estimates and a trial choice for  $\alpha(P=0)$ , corresponding values of  $\Delta F(0)$ ,  $\gamma(0)$ , and  $f_v$  are found that reasonably fit our observations. The fitting is repeated for new choices of  $\alpha(P=0)$ , varied over sensible limits. This allows us to explore the ranges of  $\Delta F(0)$ ,  $\gamma(0)$ , and  $f_v$  that are realistic

and also reproduce our findings for the NC precipitation in ZnSe and ZnTe.

For CdSe, where no Se NC precipitation is seen, a different strategy that makes use directly of the t-Se cohesive energy is employed, as described in the text.

- 
- [1] B. A. Weinstein, *Solid State Commun.* **24**, 595 (1977); B. A. Weinstein, in *High Pressure Science and Technology*, edited by K. D. Timmerhaus and M. S. Barber (Plenum, New York, 1979), Vol. 1, pp.141–151.
- [2] R. G. Greene, H. A. Luo, and A. L. Ruoff, *J. Phys. Chem. Solids* **56**, 521 (1995).
- [3] R. E. Tallman, G. Lindberg, B. Shih, P. Zhang, B. A. Weinstein, R. Lauck, and M. Cardona, *High Pressure Research* (Taylor & Francis, Paris, 2009), Vol. 29, pp. 476–481.
- [4] C. E. M. Campos, J. C. de Lima, T. A. Grandi, J. P. Itie, A. Polian, and A. Michalowicz, *J. Phys.-Condens. Matter* **17**, 5187 (2005).
- [5] L. D. Yao, F. F. Wang, X. Shen, S. J. You, L. X. Yang, S. Jiang, Y. C. Li, K. Zhu, Y. L. Liu, A. L. Pan, B. S. Zou, J. Liu, C. Q. Jin, and R. C. Yu, *J. Alloy Compd.* **480**, 798 (2009).
- [6] J. Camacho, I. Loa, A. Cantarero, and K. Syassen, *J. Phys.: Condens. Matter* **14**, 739 (2002).
- [7] M. D. Frogley, D. J. Dunstan, and W. Palosz, *Solid State Commun.* **107**, 537 (1998).
- [8] G. P. Lindberg, R. E. Tallman, R. Lauck, M. Cardona, X. Liu, J. K. Furdyna, and B. A. Weinstein, *Phys. Status Solidi B* **250**, 711 (2013).
- [9] T. Sander, M. S. Rinn, and P. J. Klar, *Phys. Status Solidi B* **250**, 688 (2013).
- [10] A. P. Alivisatos, T. D. Harris, L. E. Brus, and A. Jayaraman, *J. Chem. Phys.* **89**, 5979 (1988).
- [11] H. M. Fan, Z. H. Ni, Y. P. Feng, X. F. Fan, J. L. Kuo, Z. X. Shen, and B. S. Zou, *Appl. Phys. Lett.* **90**, 021921 (2007).
- [12] J. Schroeder and P. D. Persans, *J. Lumin.* **70**, 69 (1996).
- [13] Y. C. Lin, C. H. Chiu, W. C. Fan, S. L. Yang, D. S. Chuu, and W. C. Chou, *J. Appl. Phys.* **101**, 073507 (2007).
- [14] J. Camacho, I. Loa, A. Cantarero, K. Syassen, I. Hernandez-Calderon, and L. Gonzalez, *Phys. Status Solidi B* **235**, 432 (2003).
- [15] A. K. Arora, E. K. Suh, U. Debska, and A. K. Ramdas, *Phys. Rev. B* **37**, 2927 (1988).
- [16] A. K. Arora and T. Sakuntala, *Phys. Rev. B* **52**, 11052 (1995).
- [17] C. S. Yang, C. S. Ro, W. C. Chou, C. M. Lin, D. S. Chuu, J. Hu, E. Huang, and J. Xu, *J. Appl. Phys.* **85**, 8092 (1999).
- [18] C. M. Lin, D. S. Chuu, T. J. Yang, W. C. Chou, J. A. Xu, and E. Huang, *Phys. Rev. B* **55**, 13641 (1997).
- [19] J. Bak, U. Venkateswaran, C. L. Mak, R. Sooryakumar, and B. T. Jonker, *J. Phys. Chem. Solids* **56**, 563 (1995).
- [20] B. A. Weinstein and R. Zallen, in *Light Scattering in Solids IV*, edited by M. Cardona and G. Guntherodt (Springer, Berlin, 1984), Vol. 54, pp. 463–527.
- [21] D. N. Talwar, M. Vandevyver, K. Kunc, and M. Zigone, *Phys. Rev. B* **24**, 741 (1981).
- [22] T. Soma, *Solid State Commun.* **34**, 927 (1980).
- [23] A. Debernardi and M. Cardona, *Phys. Rev. B* **54**, 11305 (1996).
- [24] J. Camacho, K. Parlinski, A. Cantarero, and K. Syassen, *Phys. Rev. B* **70**, 033205 (2004).
- [25] I. Hamdi, M. Aouissi, A. Qteish, and N. Meskini, *Phys. Rev. B* **73**, 174114 (2006).
- [26] E. Deligoz, K. Colakoglu, and Y. Ciftci, *Physica B* **373**, 124 (2006).
- [27] J. J. Tan, G. F. Ji, X. R. Chen, and Q. Q. Gou, *Commun. Theor. Phys.* **53**, 1160 (2010).
- [28] H. Y. Wang, J. Cao, X. Y. Huang, and J. M. Huang, *Condens. Matter Phys.* **15**, 13705 (2012).
- [29] S. Saib, M. A. Khan, and N. Bouarissa, *Physica B* **407**, 3570 (2012).
- [30] M. Cote, O. Zakharov, A. Rubio, and M. L. Cohen, *Phys. Rev. B* **55**, 13025 (1997).
- [31] J. R. Chelikowsky, *Phys. Rev. B* **35**, 1174 (1987).
- [32] G. D. Lee and J. Ihm, *Phys. Rev. B* **53**, R7622(R) (1996).
- [33] A. Qteish and A. Munoz, *J. Phys.-Condens. Mat.* **12**, 1705 (2000).
- [34] S. Alptekin, *J. Mol. Model* **18**, 1167 (2012).
- [35] K. Sarasamak, S. Limpijumngong, and W. R. L. Lambrecht, *Phys. Rev. B* **82**, 035201 (2010).
- [36] D. Kirin and I. Lukacevic, *Phys. Rev. B* **75**, 172103 (2007).
- [37] T. Basak, M. N. Rao, M. K. Gupta, and S. L. Chaplot, *J. Phys.-Condens. Matter* **24**, 115401 (2012).
- [38] J. Pellicer-Porres, D. Martinez-Garcia, C. Ferrer-Roca, A. Segura, V. Munoz-Sanjose, J. P. Itie, A. Polian, and P. Munsch, *Phys. Rev. B* **71**, 035210 (2005).
- [39] J. Pellicer-Porres, A. Segura, V. Munoz, J. Zuniga, J. P. Itie, A. Polian, and P. Munsch, *Phys. Rev. B* **65**, 012109 (2002).
- [40] M. I. McMahon and R. J. Nelmes, *Phys. Status Solidi B* **198**, 389 (1996).
- [41] R. J. Nelmes, M. I. McMahon, N. G. Wright, and D. R. Allan, *J. Phys. Chem. Solids* **56**, 545 (1995); M. I. McMahon and R. J. Nelmes, *ibid.* **56**, 485 (1995).
- [42] A. San Miguel, A. Polian, M. Gauthier, and J. P. Itie, *Phys. Rev. B* **48**, 8683 (1993).
- [43] S. Leoni, R. Ramlau, K. Meier, M. Schmidt, and U. Schwarz, *Proc. Natl. Acad. Sci. U.S.A.* **105**, 19612 (2008).
- [44] A. Ohtani, M. Motobayashi, and A. Onodera, *Phys. Lett. A* **75**, 435 (1980).
- [45] A. Mujica, A. Rubio, A. Munoz, and R. J. Needs, *Rev. Mod. Phys.* **75**, 863 (2003).
- [46] R. J. Nelmes and M. I. McMahon, in *Semiconductors and Semimetals*, edited by S. Tadeusz and P. William (Elsevier, Amsterdam, 1998), Vol. 54, pp. 145–246.
- [47] J. M. Besson, J. P. Itie, A. Polian, G. Weill, J. L. Mansot, and J. Gonzalez, *Phys. Rev. B* **44**, 4214 (1991).
- [48] W. C. Chou, C. M. Lin, R. S. Ro, C. S. Ho, D. Y. Hong, C. S. Yang, D. S. Chuu, T. J. Yang, J. Xu, and E. Huang, *Chin. J. Phys.* **35**, 266 (1997).
- [49] D. S. Chuu and C. M. Lin, *Chin. J. Phys.* **35**, 509 (1997).

- [50] Z. Lilientalweber, X. W. Lin, J. Washburn, and W. Schaff, *Appl. Phys. Lett.* **66**, 2086 (1995).
- [51] C. E. M. Campos and P. S. Pizani, *J. Appl. Phys.* **89**, 3631 (2001).
- [52] J. H. Huang, W. N. Lee, X. J. Kuo, and Y. O. Su, *J. Phys. Condens. Matter* **18**, 3897 (2006).
- [53] M. N. Chang, K. C. Hsieh, T. E. Nee, C. C. Chuo, and J. I. Chyi, *J. Cryst. Growth* **201**, 212 (1999).
- [54] S. Fleischer, C. D. Beling, S. Fung, W. R. Nieveen, J. E. Squire, J. Q. Zheng, and M. Missous, *J. Appl. Phys.* **81**, 190 (1997).
- [55] G. A. Kulkarni, V. G. Sathe, K. S. R. K. Rao, D. V. S. Muthu, and R. K. Sharma, *J. Appl. Phys.* **105**, 063512 (2009).
- [56] W. Palosz, D. Gillies, K. Grasza, H. Chung, B. Raghathamachar, and M. Dudley, *J. Cryst. Growth* **182**, 37 (1997).
- [57] J. W. Cahn, *Acta Metall.* **5**, 169 (1957).
- [58] F. R. N. Nabarro, *Theory of Crystal Dislocations* (Dover, New York, 1987), Chap. 6, especially pp. 474–481, and references therein.
- [59] R. Lauck and E. Schonherr, *J. Cryst. Growth* **197**, 513 (1999); see also R. Lauck, *ibid.* **312**, 3642 (2010).
- [60] J. Fan, L. Ouyang, X. Liu, D. Ding, J. K. Furdyna, D. J. Smith, and Y. H. Zhang, *J. Cryst. Growth* **323**, 127 (2011).
- [61] N. Samarth, H. Luo, J. K. Furdyna, S. B. Qadri, Y. R. Lee, A. K. Ramdas, and N. Otsuka, *Appl. Phys. Lett.* **54**, 2680 (1989).
- [62] S. Ves, K. Stroessner, N. E. Christensen, C. K. Kim, and M. Cardona, *Solid State Commun.* **56**, 479 (1985).
- [63] B. A. Weinstein, R. Zallen, M. L. Slade, and A. deLozanne, *Phys. Rev. B* **24**, 4652 (1981).
- [64] W. Shan, W. Walukiewicz, H. W. Ager III, K. M. Yu, J. Wu, and E. E. Haller, *Appl. Phys. Lett.* **84**, 67 (2004); Note that we use the pressure coefficients for wurtzite CdSe in TABLE I along with  $E_g(1 \text{ atm}) = 1.67 \text{ eV}$ , the observed band gap of zincblende CdSe at 1 atm given in Ref. [61].
- [65] S. Kamran, K. Y. Chen and L. Chen, *Phys. Rev. B* **77**, 094109 (2008).
- [66] P. Tomasini, A. Haidoux, M. Maurin, and J. C. Tedenac, *J. Cryst. Growth* **166**, 590 (1996).
- [67] We are not concerned here with the higher-pressure transitions and phases; see Ref. [45] for a summary.
- [68] R. J. Angel, M. Bujak, J. Zhao, G. D. Gatta, and S. D. Jacobsen, *J. Appl. Crystallogr.* **40**, 26 (2007).
- [69] R. Kremer, M. Cardona, R. Lauck, G. Siegle, and A. Romero, *Phys. Rev. B* **85**, 035208 (2012).
- [70] J. C. Irwin and J. LaCombe, *J. Appl. Phys.* **41**, 1444 (1970).
- [71] R. G. Alonso, E. K. Suh, A. K. Ramdas, N. Samarth, H. Luo, and J. K. Furdyna, *Phys. Rev. B* **40**, 3720 (1989).
- [72] F. Widulle, S. Kramp, N. M. Pyka, A. Göbel, T. Ruf, A. Debernardi, R. Lauck, and M. Cardona, *Physica B* **263**, 448 (1999).
- [73] P. J. Dean, *Phys. Status Solidi A* **81**, 625 (1984); P. J. Dean, A. D. Pitt, M. S. Skolnick, P. J. Wright, and B. Cockayne, *J. Cryst. Growth* **59**, 301 (1982).
- [74] J. L. Patel, J. J. Davies, and J. E. Nicholls, *J. Phys. C* **14**, 5545 (1981).
- [75] M. Godlewski, W. E. Lamb, and B. C. Cavenett, *Solid State Commun.* **39**, 595 (1981).
- [76] G. D. Watkins, in *Handbook of Semiconductor Technology: Electronic Structure and Properties of Semiconductors*, edited by K. A. Jackson and W. Schroeter (Wiley-VCH, Berlin, 2000), Vol. 1, pp. 121–165.
- [77] I. Chen and R. Zallen, *Phys. Rev.* **173**, 833 (1968).
- [78] R. M. Martin, G. Lucovsky, and K. Helliwell, *Phys. Rev. B* **13**, 1383 (1976). The stable ambient phase of both Se and Te has a trigonal crystal structure. It consists of covalently bonded spiral (triad) chains of atoms arrayed in  $c$ -axis orientation on a hexagonal lattice in the  $a$ - $b$  plane. The  $A1$  mode is a cylindrical breathing oscillation in which the Se (or Te) atoms of each chain undergo motion normal to the  $c$  axis.
- [79] R. L. Schmidt, K. Kunc, M. Cardona, and H. Bilz, *Phys. Rev. B* **20**, 3345 (1979).
- [80] C. Trallero-Giner, K. Kunc, and K. Syassen, *Phys. Rev. B* **73**, 205202 (2006). The decrease in intensity of  $\text{TO}(\Gamma)$  and  $\text{LO}(\Gamma)$  arises from loss of resonance enhancement as the ZnSe band gap increases with pressure, combined with cancellations between other terms in the ZnSe Raman cross section.
- [81] W. Richter, J. B. Renucci, and M. Cardona, *Phys. Status Solidi B* **56**, 223 (1973).
- [82] A. K. Bandyopadhyay and L. C. Ming, *Phys. Rev. B* **54**, 12049 (1996).
- [83] K. Aoki, O. Shimomura, S. Minomura, N. Koshizuka, and T. Tsushima, *J. Phys. Soc. Jpn.* **48**, 906 (1980).
- [84] O. Degtyareva, E. R. Hernandez, J. Serrano, M. Somayazulu, H. K. Mao, E. Gregoryanz, and R. J. Hemley, *J. Chem. Phys.* **126**, 084503 (2007).
- [85] P. J. Carroll and J. S. Lannin, *Solid State Commun.* **40**, 81 (1981).
- [86] M. Gorman and S. A. Solin, *Solid State Commun.* **18**, 1401 (1976).
- [87] C. Marini, D. Chermisi, M. Lavagnini, D. Di Castro, C. Petrillo, L. Degiorgi, S. Scandolo, and P. Postorino, *Phys. Rev. B* **86**, 064103 (2012).
- [88] S. Wang, D. Ding, X. Liu, X. B. Zhang, D. J. Smith, J. K. Furdyna, and Y. H. Zhang, *J. Cryst. Growth* **311**, 2116 (2009).
- [89] L. Ouyang, J. Fan, S. Wang, X. Lu, Y. H. Zhang, X. Liu, J. K. Furdyna, and D. J. Smith, *J. Cryst. Growth* **330**, 30 (2011).
- [90] A. S. Pine and G. Dresselhaus, *Phys. Rev. B* **4**, 356 (1971).
- [91] Note that in ZnTe at 1 atm the  $(\text{TO-TA})(X, K)$  difference mode ( $117 \text{ cm}^{-1}$ ) lies close to the  $2\text{TA}(X)$  peak and also to the  $A1$  mode of t-Te.
- [92] The most cleanly cleaved chips were usually the chips that dispersed from pin cleaving a large as-grown sample at a single point.
- [93] J. Camacho, I. Loa, A. Cantarero, and K. Syassen, *High Press. Res.* **22**, 309 (2002).
- [94] In the ZnTe film, the cage effect can operate in the material near the GaSb substrate, leading to the bifurcated  $A1$  pressure shift seen in Fig. 7(b).
- [95] T. Suzuki, S. Takeuchi, and H. Yoshinaga, *Dislocation Dynamics and Plasticity* (Springer, Berlin, 1991), see Chaps. 5 and 7.
- [96] Shockley partial dislocations are pairs of lattice dislocations that dissociate from a parent dislocation such that the total Burger's vector is conserved. For fcc tetrahedral materials a common Burger's vector dissociation is  $[1, 0, -1]a/2 \rightarrow [2, -1, -1]a/6 + [1, 1, -2]a/6$ . In order for Shockley par-

- tials to form, the lattice develops stacking faults between the two partials. See Ref. [95], pp. 100–102.
- [97] K. H. Chow and G. D. Watkins, *Phys. Rev. Lett.* **81**, 2084 (1998).
- [98] G. M. Dalpian and S. H. Wei, *Phys. Rev. B* **72**, 075208 (2005).
- [99] H. Morkoc, S. Strite, G. B. Gao, M. E. Lin, B. Sverdlov, and M. Burns, *J. Appl. Phys.* **76**, 1363 (1994).
- [100] G. Kiriakidis, K. Moschovis, P. Uusimaa, A. Salokatve, M. Pessa, and J. Stoemenos, *Thin Solid Films* **360**, 195 (2000).
- [101] G. Horsburgh, K. A. Prior, W. Meredith, I. Galbraith, B. C. Cavenett, C. R. Whitehouse, G. Lacey, A. G. Cullis, P. J. Parbrook, P. Mock, and K. Mizuno, *Appl. Phys. Lett.* **72**, 3148 (1998).
- [102] D. Y. Jeon, H. P. Gislason, and G. D. Watkins, *Phys. Rev. B* **48**, 7872 (1993).
- [103] P. J. Dean, H. Venghaus, J. C. Pfister, B. Schaub, and J. Marine, *J. Lumin.* **16**, 363 (1978).
- [104] R. E. Tallman, A. Reznik, B. A. Weinstein, S. D. Baranovskii, and J. A. Rowlands, *Appl. Phys. Lett.* **93**, 212103 (2008).
- [105] G. P. Lindberg, T. O’Loughlin, N. Gross, A. Mishchenko, A. Reznik, S. Abbaszadeh, K. S. Karim, G. Belev, and B. A. Weinstein, *J. Appl. Phys.* **116**, 193511 (2014).
- [106] H. Luo (private communication).
- [107] C. Kittel, *Introduction to Solid State Physics*, 8th. ed. (Wiley, Hoboken, NJ, 2005), p. 50.
- [108] In ZnTe the value  $P_+ = 2.0$  GPa is chosen as a compromise between the bulk and film I results that allows for the uncertainty in determining this quantity. If the bulk ZnTe result  $P_+ = 1.5$  GPa were used, an equally good fit could be calculated with the same values of  $\Delta F(0)$  and  $\gamma(0)$ , but smaller  $f_v$  would be needed. In ZnSe the value  $P_+ = 8.8$  GPa is chosen as a plausible upper limit. Higher  $P_+$  could be adopted, but tend to drive  $\Delta F(0)$  above the CED of t-Se, and using lower  $P_+$  quickly shifts  $\alpha(0)$  too high as  $P_+$  approaches  $P_-$ .
- [109] L. I. Berger, *Semiconductor Materials*, edited by F. Shapiro (CRC, Boca Raton, FL, 1997), Chap. 3 and references therein; J. Akola and R. O. Jones, *Phys. Rev. B* **85**, 134103 (2012).
- [110] S. H. Wei and S. B. Zhang, *Phys. Rev. B* **66**, 155211 (2002).
- [111] See, e.g., *Atomic Diffusion in Semiconductors*, edited by D. Shaw (Plenum, New York, 1973), Chaps. 1 and 7.
- [112] N. V. Sochinskii, M. D. Serrano, E. Dieguez, F. Agullorueda, U. Pal, J. Piqueras, and P. Fernandez, *J. Appl. Phys.* **77**, 2806 (1995).
- [113] K. Peters, A. Wenzel, and P. Rudolph, *Cryst. Res. Technol.* **25**, 1107 (1990).
- [114] G. Simmons and H. Wang, *Single Crystal Elastic Constants and Calculated Aggregate Properties: A Handbook*, 2nd ed. (M.I.T. Press, Cambridge, MA, 1971).
- [115] For precipitation of cation NCs,  $\alpha(0)$  would need to be computed using the CED of the cation’s crystal structure. In the present discussion we are treating the case in which the metal cations diffuse away toward the surface as for Zn in ZnSe and ZnTe.
- [116] W. R. Woody and J. M. Meese, *J. Appl. Phys.* **47**, 3640 (1976).
- [117] B. A. Wilson, C. E. Bonner, R. D. Feldman, R. F. Austin, D. W. Kisker, J. J. Krajewski, and P. M. Bridenbaugh, *J. Appl. Phys.* **64**, 3210 (1988).
- [118] The assignments given here for the broad low-energy PL bands in ZnSe and ZnTe are the most likely. In both materials, PL due to recombination processes at  $A$  centers, identified as trigonally relaxed D- $V_{Zn}$  pairs, can also contribute broad bands in overlapping spectral regions. See G. D. Watkins, in *Handbook of Semiconductor Technology*, edited by W. Schroeter (Wiley-VCH, Weinheim, 1999), Chap. 3.
- [119] Y. Biao, M. Azoulay, M. A. George, A. Burger, W. E. Collins, E. Silberman, C. H. Su, M. E. Volz, F. R. Szofran, and D. C. Gillies, *J. Cryst. Growth* **138**, 219 (1994).
- [120] C. H. Henry, K. Nassau, and J. W. Shiever, *Phys. Rev. B* **4**, 2453 (1971).
- [121] P. Y. Yu and C. Hermann, *Phys. Rev. B* **23**, 4097 (1981).
- [122] Y. P. Gnatenko, P. M. Bukivskij, I. O. Faryna, A. S. Opanasyuk, and M. M. Ivashchenko, *J. Lumin.* **146**, 174 (2014).
- [123] R. Jagerwaldau, N. Stucheli, M. Braun, M. L. Steiner, E. Bucher, R. Tenne, H. Flaisher, W. Kerfin, R. Braun, and W. Koschel, *J. Appl. Phys.* **64**, 2601 (1988).
- [124] C. H. Su, S. Feth, L. J. Wang, and S. L. Lehoczky, *J. Cryst. Growth* **224**, 32 (2001).
- [125] S. Satoh and K. Igaki, *Jpn. J. Appl. Phys.* **19**, 1953 (1980); S. M. Huang, Y. Nozue, and K. Igaki, *Jpn. J. Appl. Phys.* **22**, L420 (1983).
- [126] A. Saxena, Q. Pan, and H. E. Ruda, *Nanotechnology* **24**, 105701 (2013).
- [127] S. Myhajlenko, J. L. Batstone, H. J. Hutchinson, and J. W. Steeds, *J. Phys. C* **17**, 6477 (1984).
- [128] G. B. Stringfellow and R. H. Bube, *Phys. Rev.* **171**, 903 (1968).
- [129] J. Bittebierre and R. T. Cox, *Phys. Rev. B* **34**, 2360 (1986).
- [130] G. Shigaura, M. Ohashi, Y. Ichinohe, M. Kanamori, N. Kimura, N. Kimura, T. Sawada, K. Suzuki, and K. Imai, *J. Cryst. Growth* **301**, 297 (2007).
- [131] G. Parthasarathy and W. B. Holzapfel, *Phys. Rev. B* **38**, 10105 (1988).
- [132] G. Parthasarathy and W. B. Holzapfel, *Phys. Rev. B* **37**, 8499 (1988).